R. & M. No. 3383

MINISTRY OF AVIATION

AERONAUTICAL RESEARCH COUNCIL
REPORTS AND MEMORANDA

On Lifting Bodies which Contain Two-Dimensional Supersonic Flows

By L. H. Townend

LONDON: HER MAJESTY'S STATIONERY OFFICE
1964
PRICE 18*s*. 6*d*. NET

On Lifting Bodies which Contain Two-Dimensional Supersonic Flows

By L. H. Townend

Communicated by the Deputy Controller Aircraft (Research and Development)
Ministry of Aviation

*Reports and Memoranda No. 3383**
August, 1963

Summary.

This paper is primarily concerned with the design principles of three-dimensional surfaces which can produce two-dimensional, centred compression waves and are derived from the Nonweiler wing. A study is made of the efficiencies (i.e. of the pressure recoveries) of various multi-shock and isentropic compression flows, and of the lateral slenderness of related caret bodies. For bodies producing isentropic compression, spanwise pressure distributions are shown to depend on anhedral and planform and it is noted that such bodies should be of use in research on three-dimensional boundary layers. It is shown that multi-wave and isentropic compression surfaces may be used as intakes (or isentropic bodies as nozzles), and that these can be used as components in the design of configurations, beneath which lifting and propulsive flows can be wholly two-dimensional. Various models are proposed for inclusion in current wind-tunnel programmes.

LIST OF CONTENTS

* Replaces R.A.E. Report No. Aero. 2675—A.R.C. 25 277.

LIST OF CONTENTS—*continued*

LIST OF ILLUSTRATIONS

LIST OF ILLUSTRATIONS—*continued*

Figure

---

1. *Introduction.*

For flight at subsonic and low supersonic speeds, it is possible to use aircraft shapes on which flow perturbations are everywhere fairly small compared with the flight velocity. Küchemann[1] has shown the classical aircraft configuration to be appropriate at low flight speeds, the swept wing at higher speeds, and the slender wing at Mach numbers of about 2. At higher flight speeds however, disturbances will probably not be small in all regions and may include shock waves of finite strength; aircraft for high supersonic and hypersonic speeds should therefore be based on shapes with appropriate types of flow.

To this end, Maikapar[2] and Nonweiler[3, 4] have defined a class of bodies, for which the flow disturbance is, at design conditions, a single, plane shock wave. The elemental body of this class is a delta wing of inverted-V cross-section upon which, at design conditions of Mach number and incidence, a plane, oblique shock wave attaches to the leading edges; such a shape has since been termed a 'caret wing' by various authors*.

Basic aerodynamic features have been analysed by Squire[5] and Peckham[6], the effects of yaw by Bagley[7], and boundary-layer characteristics by Catherall[8]; some experimental results have been

* The typographic term 'caret' was originally adopted to describe inverted-V anhedral forms; in this paper its use will be extended, with some regret, to those of inverted-U form.

published by Squire[9], Pennelegion and Cash[10], Sykes[11] and Treadgold[12, 1]. Bodies compounded of wedge and caret elements have been described by Waterhouse[13]. To date therefore, detailed attention has been restricted to bodies over which each component flow is compressed by a single, plane, oblique shock wave; in principle however, supersonic compression can occur through a sequence of plane, oblique shock waves, the flow between adjacent waves being uniform but at an individual value of nett deflection from the free-stream direction. Oswatitsch[14] has studied the efficiency of such shock combinations and has shown that, for the nett loss in stagnation pressure (or rise in entropy) to be a minimum, successive shock waves should be of equal strengths. In the extreme case, the number of shock waves may be made infinite, so that individual strengths become infinitesimal and nett stagnation-pressure losses zero; compression is then isentropic and may be produced for example by a reversed Prandtl-Meyer expansion wave.

Such a wave can of course be produced by a simple, two-dimensional wedge, but at the Royal Aircraft Establishment an initial study has been made of the design principles and likely characteristics of bodies which can produce two-dimensional compression (or expansion) flows, but which are themselves three-dimensional and derive from the Nonweiler wing; the existence of such bodies has been noted recently by Flower[15] and by Southgate and Pedersen[16]. In this paper, design principles are described for bodies based on the reversed Prandtl-Meyer expansion wave (but the relevance of the general principle to other flows is noted). Since isentropic processes involve no stagnation-pressure losses, the isentropic variant of the Nonweiler wing may be treated as a 'reference body', against which the merits of others may be judged; on this basis the efficiencies, i.e. the pressure recoveries, of various isentropic and multi-shock wave systems are assessed, together with geometric features of related caret bodies. For isentropic bodies themselves, the manner in which the pressure distribution on the compression surface depends on planform and anhedral is described, and on the basis of boundary-layer considerations, tentative suggestions for further study are made.

Bodies of the type described in this paper are shown to be well suited for research on three-dimensional boundary layers, and for use as intakes and nozzles; further by use of the same principle, realistic configurations may be designed for aircraft beneath which lifting and propulsive flows are fully integrated and at design conditions, wholly two-dimensional.

Finally, it should be noted that multi-shock and isentropic compression is not restricted to two-dimensional flow, and might, for example, be considered for lifting bodies derived from the flows of non-lifting cones[17, 18].

2. *Design Principles of Caret Bodies.*

At design conditions, an inverted-V Nonweiler wing produces a single, plane, oblique shock wave lying between the leading edges (*see* Fig. 1a). More complex bodies may be compounded from this basic 'flow-plus-body' element, for example the Maikapar body[2]; however, each component flow is individually analogous with that over an infinite wedge in a uniform, supersonic stream (*see* Fig. 1b), or more realistically with that of a single wedge with sidewalls (*see* Fig. 1c). To date, Nonweiler bodies have been thought of primarily as lifting surfaces, but since the wedge with sidewalls is a typical form of supersonic intake, such bodies are clearly appropriate, in principle, as intakes (or other component parts of a vehicle); further, the requirement for sidewalls on the analogous wedge intake serves to emphasise that the caret body provides a 'contained' flow, despite its relatively open structural form.

2.1. *The Caret Body Producing a Single Shock Wave.*

For a Nonweiler wing at a given free-stream Mach number, a prescribed shock-wave static-pressure ratio (or undersurface pressure coefficient) will correspond to a particular shock-wave angle and flow deflection (ζ and δ in Fig. 2a); the latter determines the lower ridge line, the lower surface of the body is defined by streamlines of which S in Fig. 2a is typical, and for flow containment, the leading edges of the body are defined to lie in the plane of the shock wave.

An infinite number of body surfaces can be defined in this way, any one of which can be specified, either by the trace of the leading edges in the shock plane, or by definition of the tip-line and the lateral limits of the 'capture flow tube' (enclosing that air which will be momentarily contained beneath the body). If the leading-edge traces are straight lines, then as seen in Fig. 2b they define a capture flow tube of triangular cross-section; hence, for the related caret body of Fig. 2c, a certain constant anhedral must result.

It is clearly permissible to define curved leading-edge traces in the shock plane, and consequently, non-triangular capture flow tubes; the body having a semi-circular flow tube and hence non-uniform anhedral distribution, is sketched in Fig. 2d, and in the more detailed 'summary' Fig. 3. It is seen that a full design requires only the definition of

(1) the cross-section of the capture flow tube (in which choice there is virtually complete freedom apart from, for example, planform restrictions due to low-speed considerations), and

(2) the equivalent-wedge flow model (which must avoid shock detachment for the given free-stream Mach number and, by determining the strength of the shock, will define the flow conditions beneath the body and the efficiency with which compression is achieved).

In the analogous case of two-dimensional, supersonic intakes using shock waves for external compression, the efficiency (as measured by the overall stagnation pressure ratio) can be improved by using a sequence of shock waves for compression. This technique, as applied to caret bodies, is now examined.

3. *The Isentropic Caret Body.*

For a multi-shock wave system producing compression of a given supersonic stream, Oswatitsch[14] has shown that losses in stagnation pressure will fall as the number of shock waves is increased and that, for minimum loss, these component shock waves should be of equal strengths; in the limit, supersonic compression can be made isentropic by use of an infinite number of infinitely weak compression waves. In two-dimensional flow this could correspond to a reversed form of the Prandtl-Meyer expansion wave, i.e. to the isentropic, centred compression wave.

For some applications, fully isentropic compression may be less desirable than a multi-shock system; however, design principles of related caret bodies are identical.

3.1. *The Reversed Prandtl-Meyer Expansion Wave.*

The Prandtl-Meyer wave for supersonic expansion of an airflow around a two-dimensional corner is shown in Fig. 4a. A uniform airstream originally flowing without friction and at sonic speed along a flat wall W, expands supersonically downstream of the sonic line at a corner C, from which radiates a 'fan' of straight, infinitely weak expansion waves (identical with the characteristic lines). The flow angle ν increases as expansion proceeds, but this and other flow properties are constant along a given wave. Any streamline S (originally at distance 'd' from the wall W) may of course be replaced by a solid boundary shown as AB in Fig. 4b.

Expansion is complete when the static pressure of the flow falls to that of the discharge region, and downstream of the final characteristic (which is inclined to the discharge flow at an angle, $\sin^{-1} 1/M_{\text{exp}}$) the jet boundary will be straight and parallel to the final direction of AB.

If the flow is now reversed so that a uniform stream of Mach number $M_\infty (= M_{\text{exp}}$ in Fig. 4b) flows into some part of the original (expansion) surface, say BDE in Fig. 4c, then the characteristic lines will now represent compression waves propagated across the flow; wave [1] inclines to the free stream at the characteristic angle, $\sin^{-1} 1/M_\infty$, and all waves are focussed at a point corresponding to C in Fig. 4b. Since this isentropic wave produces two-dimensional centred compression of an originally uniform free stream, the compressed flow emerges (at a reduced Mach number, M_{comp}) with uniform properties. This is the reversed Prandtl-Meyer expansion wave.

In the practical case, a body such as that of Fig. 4c would be rejected due to the infinitesimal apex angle. If volume cannot be added to the upper surface, then by the addition of a single shock wave, the flow can be modified to that of Fig. 4d; the oblique shock wave will now involve some loss in stagnation pressure, but the overall length of the compression surface is reduced, the apex angle increased to a finite value and further compression, from the reduced Mach number M_∞', will be isentropic. Note that, for centred compression the shock wave must pass through the focal point so that the initial compression wave must be propagated at some finite distance downstream of the shock; part of the surface behind the leading edge must therefore be plane.

The use of such flow models for the design of low-loss variants of the Nonweiler wing is now discussed.

3.2. *The Design of Isentropic Caret Bodies.*

The design principles of the isentropic caret body are most simply demonstrated by deriving such a body, by the wedge flow analogy, directly from the Nonweiler wing.

Consider in Fig. 5a the body which has a delta planform and triangular capture flow tube, and is derived from a flow model identical with that of the wedges (with sidewalls) of Fig. 5b. Suppose now that the latter bodies are compounded to form the 'stepped wedge' of Fig. 5c. Clearly, since there are identical flows beneath each wedge, removal of the stippled sidewall in Fig. 5c will not modify the flow; if now the number of 'steps' is increased, the 'stepped caret' body of Fig. 5d can be produced, provided that each wedge corresponds to a chosen streamline in Flow Model I so that each is set at the same inclination to the free stream and all leading edges are co-planar. Finally, as observed in Fig. 5d', this body can revert to the Nonweiler inverted-V wing if, at a given span, the step width d tends to zero.

Suppose now that the simple-wedge Flow Model I is replaced by a centred compression wave, Flow Model II in Fig. 5e, in which streamlines A', B' and C' are typical, and for which the focal point is F. Clearly, by selection of particular streamlines from this model, it is again possible to define compression surfaces of a 'stepped caret' body, although this will now contain a two-dimensional wave producing isentropic compression. Further, by choosing streamlines on either side of A', B' C', extra component wedges may be defined and, if this process is continued indefinitely (so that steps between wedges become infinitesimal), then the body will again revert to an inverted-V caret body but, as shown in Fig. 5f, to a version producing centred, isentropic compression.

Some geometric properties of isentropic bodies immediately follow. Firstly, if waves [1] and [2] determine the initial and discharge planes of the contained flow and so the leading- and trailing-edge

planes of the caret body, then their line of intersection locates not only the focal line of the compression wave but the tips of all possible bodies. Secondly, since at any spanwise station the contour of the compression surface is that of a streamline in the relevant Prandtl-Meyer wave, then chordwise sections at all stations across the span are geometrically similar; thus any local dimension differs from the corresponding dimension on the root section in proportion as the ratio (local chord/root chord).

In summary then, design conditions for a caret body producing contained, centred, isentropic compression are as follows:

(1) the leading and trailing edges must be aligned in the planes of the chosen initial and discharge compression waves,

(2) the focal line of the compression wave must pass through the tips,

(3) streamwise sections of the compression surface must correspond to particular streamlines in the relevant Prandtl-Meyer wave and so, must be geometrically similar.

The above conditions require no reference to the geometry of the capture flow tube and so, as in Section 2.1, a specific body can be chosen from an infinite variety by defining, for a given flow model, either the leading- (or the trailing-) edge trace or the capture flow tube (*see* Fig. 6a). However, for the particular case of the body for which leading and trailing edges are straight, lines drawn through corresponding points on other (geometrically similar) chordwise sections must also be straight and hence the compression surfaces of this body are conical and can be generated by straight lines radiating from the tips; this last feature is illustrated by the model of Fig. 6b. Both Figs. 6a and 6b show that, as implied in earlier figures, bodies will normally be of arrowhead planform instead of the delta form usually assumed for Nonweiler wings.

Comments on these two features are made in the two closing sections.

3.2.1. *Isomorphic properties.*—For the conical surfaces of the model of Fig. 6b, a single pair of straight lines has been taken to represent the leading and trailing edge of each half-span and so (for the defined flow model, tip position and focal line) to define a triangular capture flow tube and inverted-V anhedral. If however the capture flow tube is not to be triangular, leading and trailing edges will no longer be straight lines, but at all stations across the span of any body, they must still lie in the planes of wave [1] and [2] respectively. For any chordwise section there is therefore a pair of lines (for example BG and DG in Fig. 7a), which pass through the tip-line and the leading and trailing edges of the root section, and upon which are located the leading and trailing edges of this chordwise section, that is

$$\left(\frac{r_{\text{comp}}}{r_\infty}\right)_1 = \left(\frac{r_{\text{comp}}}{r_\infty}\right)_2 = \left(\frac{r_{\text{comp}}}{r_\infty}\right)_3 = \ldots = \left(\frac{r_{\text{comp}}}{r_\infty}\right)_{\text{root}}.$$

Also, for a given chordwise section, the contour of the compression surface is given in terms of the local value of r and ϕ (*see* Fig. 7a) by the Prandtl-Meyer relation,

$$\left(\frac{r}{r_\infty}\right)_{\text{local}} = \frac{\cos^{1/k^2} k\phi_\infty}{\cos^{1/k^2} k\phi_{\text{local}}}, \text{ in which } k^2 \left(\equiv \frac{\gamma - 1}{\gamma + 1}\right) \text{ is known*;}$$

* Under some flight conditions of course, γ and hence k may vary during compression, due to the rise in static temperature—such effects are neglected here.

thus for a given free-stream Mach number, and thus a given value of ϕ_∞, $(r/r_\infty)_{\text{local}}$ is simply a function of ϕ_{local} and, in the plane of a given compression wave, is constant across the span. So, as shown in Fig. 7b:

(1) the capture flow tube and initial, discharge and intermediate compression waves are isomorphic (i.e. they are all triangular, all parabolic or all hyperbolic, etc.);

(2) the capture flow tube and hence the leading- and trailing-edge anhedral distributions are similarly isomorphic, since the latter are defined by projecting waves [1] and [2] normal to the free stream;

(3) the planform, defined as the area enclosed by downward projection of the waves [1] and [2] on to some appropriate reference plane, is again enclosed by arcs of the same geometric nature as the sides of the capture flow tube—in the case of planform however, some adaptability is available as follows.

3.2.2. *Comments on planform adaptability.*—As noted above, bodies which 'contain' isentropic, centred compression waves are normally of arrowhead planform; if however

$$A = \nu_\infty - \nu_{\text{comp}} + \mu_{\text{comp}} = \frac{\pi}{2}, \text{ then}$$

the discharge wave is normal to the free-stream direction and a delta planform is obtained. Further if $A > \pi/2$, a rhombic planform will result.

For given free-stream conditions, bodies which conform to the above relation would produce obligatory discharge values of pressure and Mach number; to avoid this restriction, and yet retain some flexibility in choice of planform, the flow model of, for example, Fig. 4c can be modified to that of Fig. 8a. Here, the Prandtl-Meyer contour is lengthened by a straight skin extension, aligned with the existing discharge flow, so that this may continue downstream at the required value of M_{comp}, but now as a uniform flow. The length of this extension can be varied arbitrarily across the span, and so as in Fig. 8b and 8c, bodies of delta or other planform may be simply produced.

4. *Some Aerodynamic Features of Caret Bodies Producing Centred Compression.*

To date, study of caret bodies has been restricted, somewhat arbitrarily, to those with straight leading edges and delta planforms. However for bodies producing isentropic, centred compression, some guidance on planform selection can be obtained by reference to possible boundary-layer conditions; this is examined in Section 4.1.

The interaction with the free stream of a contained compression wave (multi-shock or isentropic) is briefly studied in Section 4.2, and finally, in Section 4.3, the interdependence of the efficiency and flow geometry of centred compression waves and hence of related bodies.

4.1. *Pressure Distributions on Isentropic Caret Bodies.*

Since isentropic compression introduces a continuous rise in static pressure along the chord of a compression surface, the boundary layer is thereby exposed to an adverse pressure gradient and so, particularly in conditions of laminar flow, is liable to separate. However, for a caret body, isobars on the compression surface will be swept, as seen for example in Figs. 6 and 7, so that chordwise pressure gradients will be accompanied by spanwise gradients. It follows immediately that across the compression surface of an isentropic caret body, pressure gradients will have finite components

normal to the local streamline directions of the contained flow, and thus that cross-flows will be generated in the boundary layer: but it is known[19] that the existence of cross-flows can prevent boundary-layer separation and thus, for isentropic compression, caret bodies may be preferable to conventional wedges with sidewalls. Certainly, as bodies over which the flow outside the boundary layer remains two-dimensional, they would offer a simple basis for experimental or analytic study of three-dimensional boundary layers in supersonic flow; furthermore, as will now be shown, they offer considerable flexibility in design.

Consider for example, an inverted-V body producing isentropic, centred compression between inflow and discharge Mach numbers of (say) 7 and 4, and having some arbitrary value of anhedral; the root section, basic flow model and root chordwise pressure distribution are shown in Fig. 9a. Since this body has its leading and trailing edges defined by the limiting isobars, pressure and Mach number distributions will be as in Fig. 9b, and isobar sweep angle will clearly depend on the chosen planform (and so upon anhedral). For the body of Fig. 10a, these pressure distributions are illustrated in Fig. 10b, or more conventionally as chordwise and spanwise pressure distributions in Figs. 10c and 10d; these are intended to be illustrative only and in Fig. 10d, the nearly linear spanwise pressure distributions should not be regarded as typical. However from Figs. 9 and 10 it may be concluded that, for inverted-V bodies producing isentropic, centred compression,

(1) the adverse chordwise pressure gradients become infinite at the tips, so that shock waves and/or separation of the boundary layer may occur in these regions (features of shock-wave structure will be discussed in Section 4.2), and

(2) at a given chordwise station, static pressure decreases across the span and at the tips, gradients again become infinite—but these spanwise gradients can be favourable in that they produce outward cross-flows in the boundary layer and so can prevent boundary-layer separation, or at least can restrict separation to regions near the tips.

The magnitude and shape of these spanwise pressure gradients in fact depend on the anhedral angle and the free-stream Mach number. For example in Fig. 11, the flow model, root section and root pressure distribution of Fig. 9 are shown again, together with spanwise pressure distributions and body sections for an arrowhead body (Body A), at chordwise stations corresponding to various values of flow Mach number at the root. The pressure distributions have been constructed graphically, simply by identifying those isobars which correspond to chosen points across a given chordwise station, and so, by reference to the root pressure distribution, observing the local pressure levels; it follows that pressure distributions at chordwise stations on, for example, the more slender Bodies B and C, must be identical with the corresponding distributions on Body A, except that they extend over local spans which are reduced in the ratios S_B/S_A and S_C/S_A respectively. Thus, for inverted-V bodies which have equal root chords and produce isentropic, centred compression between the same two Mach numbers, an increase in anhedral increases the gradients of the spanwise pressure distributions but leaves unchanged their geometric nature.

This conclusion does not depend on the particular combination of Mach numbers chosen and hence applies for example to bodies designed for $M_\infty = 3$ (*see* Fig. 12); the main feature of this figure is that, at this reduced free-stream Mach number, spanwise pressure distributions become markedly convex as compression proceeds {note also that for the chosen M_{comp}-value of 1·25, the planform is rhombic, i.e. $(\nu_\infty - \nu_{\text{comp}} + \mu_{\text{comp}}) > \pi/2$}. In both Figs. 11 and 12 however, spanwise body sections are seen to be curved across the compression surface. Thus for consideration of the boundary layers of the contained flows, any spanwise pressure distribution should strictly be defined

in terms of the 'spanwise arc length' rather than the projected length; it will then depend on both the anhedral and the section curvature, which for consideration of a range of bodies might in turn be influenced by specified 'family' conditions*. Note also that planforms with equal root chords become increasingly slender as anhedral is increased so that, at a defined chordwise station, this arc length is gradually reduced; the effects of section curvature are in the opposite sense but, while these become increasingly significant as anhedral is increased, they do not appear to reverse the trend.

For the bodies considered above, the design of pressure distributions is in part controllable; however a simultaneous requirement for inverted-V anhedral and for centred compression clearly inhibits flexibility in the design of the overall pressure field, and while boundary-layer characteristics should be predictable[20, 21], adequate modification in the light of analysis may not be possible. If these requirements can be relaxed however, two possible techniques may become important: the first is to redistribute the pressure across the span of the compression surface (but as will be shown in Section 4.1.1, this depends on discarding inverted-V anhedral forms): the second, briefly examined in Section 4.1.2, involves 'cropping' the tips of an existing body, thereby to eliminate compression surfaces exposed to the more extreme adverse pressure gradients and to the tip shock system. If under some conditions, neither technique is adequate, then for pressure gradients exceeding a tolerable maximum, further compression might be produced by a non-centred wave or with boundary-layer control; these techniques are not examined in this paper.

4.1.1. *The interdependence of planform and spanwise pressure distribution.*—If spanwise pressure distributions on the compression surfaces of isentropic caret bodies are to be modified from those of Fig. 11, the flow models and root pressure distributions may still be defined as before, but arrowhead planforms and inverted-V anhedrals will no longer be obtained. Now for the flow model of Fig. 13a it has been shown in Fig. 11 that, at station S_1 for example, a nearly linear spanwise pressure distribution will result; if this is replaced by a convex spanwise pressure distribution, the local leading edge must still coincide with the point at which $\Delta p/p_\infty$ is zero, and since the pressure at a point P (say) is equal to that at a point Q on the root chord, a single isobar must pass through P and Q, although its path is so far not defined. The particular chordwise pressure distribution through P is also not defined and in principle could be provided by any one of the randomly selected pressure distributions of Fig. 13b, depending on the local chord length. However, it is known (from Section 3.2.1 and Fig. 7) that at any spanwise station the local leading and trailing edges must be related in position, such that, for P in Fig. 13c,

$$\frac{l_1}{l_2} = \frac{\mathrm{TT'}}{\mathrm{LT'}};$$

(that is, at any spanwise station on a caret body producing isentropic, centred compression, the two straight lines joining, firstly, the local and root leading edges, and secondly, the local and root trailing edges, must intersect one another on the tip-line). It follows that, for a specified pressure level to be produced at P by a chordwise pressure distribution related to those of Fig. 13b, a unique value of chord will be determined; thus, by defining the whole spanwise pressure distribution across that station, a unique planform will be defined, inboard of the line LT (*see* Figs. 13c and 13d).

* Different cases may arise according to the application; a particular case for supersonic intakes is briefly considered in Section 5.1.

In Fig. 13d, the process of raising the pressure at P is seen to depend on an outward movement of the point X, for example to X′, and thus to impose an increased chord length through P and a forward shift of the leading and trailing edges of the compression surface. It follows that the related planform of the modified isentropic body will resemble a 'curved arrowhead' or, if the corner flow along the lower ridge line is also eliminated, leading and trailing edges may be formed as continuous curves from tip to tip; possible examples of bodies based on elliptic forms are shown in Fig. 14. For a given span, the increase in pressure at a particular point has clearly increased the outboard pressure gradients (at the expense of those inboard). Cross-flows in the outboard regions may therefore be increased and since it is there that the more extreme adverse chordwise gradients exist, such a redistribution of the available pressures may be favourable; however, the curvature of spanwise body sections is clearly very pronounced and, while this could perhaps improve structural characteristics of such bodies, the effects of pressure redistribution on boundary-layer behaviour become more complicated.

However, in summary:

(1) for a caret body producing isentropic, centred compression between given values of inflow and discharge Mach number, in order to define the entire undersurface pressure field between the root and some chosen spanwise station (i.e. between $|y|/S = 0$ and $|y|/S = K$) and so to define between these stations both planform and anhedral distribution, it is only necessary to define the pressure distribution along a single line which cuts the chord lines at the root and the chosen spanwise station (such a line could correspond, as in the examples, to a constant value of x, but could as well be an isobar, or some other line);

(2) to increase the pressure on some part of the compression surface of a given caret body, the local chord lengths through that part must be increased and both the leading and the trailing edges moved upstream.

The maximum extent to which the planform may be designed by definition of a single spanwise pressure distribution is of course ABCD in Fig. 15, where B is the root trailing edge. The design of the tip region would then depend on the spanwise pressure distribution further outboard which might be chosen after analysis of boundary-layer characteristics beneath ABCD; a region CDEF might then be designed and by steps, the entire tip.

The above arguments suggest that, in preference to an examination of boundary-layer characteristics of isentropic bodies with inverted-V anhedral, it may be more realistic to investigate the interdependence of cross-section shape, planform and boundary-layer behaviour and in particular to check whether considerations of boundary-layer development would favour certain types of planform and anhedral.

4.1.2. *Caret bodies with 'cropped tips'.*—For any form of cropped caret body, the loss of the tip means that the focal line of a centred compression wave is no longer contained by structural components, so that in the tip region a more complex interaction will occur between the free stream and the 'contained' flow. One extreme type of cropping (*see* Fig. 16a) would be aimed at eliminating all sections upon which pressure gradients would be excessively adverse, but apart from spillage effects at the tip, M_{comp} would be uniform across the remaining part of the trailing edge; a second extreme type (*see* Fig. 16b) would gradually reduce the nett chordwise pressure rise from the full value at the root chord to zero at the new tip—with this method then, M_{comp} and $\Delta p/p_\infty$ would vary across the trailing edge.

Since these and other types of cropping are aimed at the prevention of boundary-layer separation, other methods such as boundary-layer control, planform redesign or non-centred compression should be considered in any particular application; however, a detailed comparison would require prediction of super- or hypersonic three-dimensional boundary layers and is not considered further in this paper.

4.2. *The Interaction of a Centred Compression Flow with a Free Stream.*

A compression flow of n centred shock waves as in Fig. 17a (or an isentropic wave as in Fig. 17b) would normally produce, by interference with the free stream at the focal point, a coalescent shock wave S and in general, due to the different conditions of the flows discharged by S and the compression flow, a reflected (expansion or compression) wave W, and a shear layer L; for the latter to be in equilibrium adjacent flows must have equal static pressures and, if viscous growth of the shear layer is negligible, identical flow directions. The shock wave S becomes, at extreme conditions, locally normal, so that the maximum possible value of the static pressure on each side of the shear layer is that behind a free-stream normal shock wave; consequently, if the presumed flow is to exist, there is a limit to the degree of compression which can be produced by either body of Fig. 17, i.e. each compression flow is subject to a turning limit. If S is to remain oblique, this limit will of course be more restrictive.

An experimental study of a flow related to that of Fig. 17b has been described by Connors, Woollett and Blue[22]. A two-dimensional body comprising a wedge (6 degrees) combined with an isentropic ramp was designed to produce, at a Mach number of 3, a centred compression wave with an overall rise in static pressure equal to that through a free-stream normal shock; in a 4×10 inch wind tunnel, at a Mach number of 3 and a Reynolds number of $2{\cdot}4 \times 10^6$ per foot, the resulting flow contained,

(a) a coalescent shock (which was not normal but corresponded to the strong oblique branch of the shock polar for that Mach number),

(b) a reflected (shock) wave from the focal line*, and

(c) a shear layer which, at these test conditions, was rather thick and grew as would a boundary layer, thereby producing a displacement effect.

For supersonic flows over caret bodies producing centred compression and operating near the turning limit, strong oblique shock waves and shear layers subject to viscous growth will probably occur; even when far removed from the turning limit, flows may still contain shear layers subject to viscous growth, so that reflected expansion waves are likely to be weakened or converted to shock waves, or an existing shock wave strengthened. In view of this, an early analysis by Johannesen[23], excluding viscous effects and using Busemann's power series for weak shock waves may well be inadequate, and the validity of a graphical (i.e. shock polar) study by Connors and Meyer[24], in which strong-shock solutions are confirmed, may be limited qualitatively due to the neglect of viscous growth in the shear layer. With these qualifications, the results of these analyses suggest that, above a certain Mach number (quoted as 2·54 in Ref. 23 and as about 3·5 in Ref. 24), the reflected wave in an isentropic flow such as Fig. 17b will be an expansion.

* Note that in these tests the presence of an expansion (such as the expansion E in Fig. 17b) is likely to have produced some weakening of the reflected shock wave.

A study to include the effects of viscosity on flows formed at hypersonic Mach numbers by centred compression systems could stem from that of Eminton[25] and also, depending on a better understanding of intended applications, a study of shock structures could perhaps be useful. Figs. 18a and 18b show cross-sections of flows which may be expected and Fig. 18c, a tentative conclusion for that of a complete caret body.

4.3. *The Flow Compactness and Efficiency of Centred Compression Waves.*

If a Nonweiler wing operates with a given combination of inflow and discharge Mach number (M_∞ and M_{comp}), then the shock inclination $(\zeta)_{n=1}$, and hence the shock strength, are thereby determined; the side elevation of such a body can then be partly defined by the lateral slenderness ratio,

$$-\left(\frac{x}{z}\right)_{\text{focus}} = \cot\zeta = \sqrt{\left\{\left(\frac{M_\infty}{(M_N)_{n=1}}\right)^2 - 1\right\}}.$$

If this single shock wave is now replaced by two of equal strength, which produce in combination the same discharge Mach number, then $(M_N)_{n=2} < (M_N)_{n=1}$ and $(\zeta_1)_{n=2} < (\zeta)_{n=1}$; however, for the same spans and capture areas, z_{focus} must be the same for each and thus the value of x_{focus} must be greater—

$$-\left(\frac{x}{z}\right)_{\text{focus}} = \cot(\zeta_1)_{n=2} = \sqrt{\left\{\left(\frac{M_\infty}{(M_N)_{n=2}}\right) - 1\right\}}.$$

On this comparison, the lateral slenderness ratio and root chord of a body increase with the number of equal shock waves it produces—hence the longest (and most slender) will be the isentropic body, for which

$$-\left(\frac{x}{z}\right)_{\text{focus}} = \underset{M_N \to 1}{\text{Lt}} \left[\sqrt{\left\{\left(\frac{M_\infty}{M_N}\right)^2 - 1\right\}}\right] = \sqrt{(M_\infty{}^2 - 1)} = \cot\mu_\infty.$$

Note that, in this case, the increment in Mach number is irrelevant since $M_N = 1$; the isentropic slenderness ratio is therefore a function of free-stream Mach number only.

A random example of the variation with n of body shape is illustrated in Fig. 19. For inflow and discharge Mach numbers of 9 and 6 respectively, a Nonweiler wing has a lateral slenderness ratio 3·52 and, for streamwise upper surfaces, a leading-edge angle of 11 degrees approximately (measured parallel to the xOz plane). As n increases, bodies producing centred compression become increasingly slender and have sharper leading edges; a maximum lateral slenderness ratio of 8·944 is reached for isentropic centred compression, together with a zero leading-edge angle. For this to be made acceptable structurally, the upper surface near the leading edge could be inclined downwards (but this region would then produce a negative lift force); alternatively, the leading-edge region of the compression surface could be converted to a shallow wedge, so as to produce the partly isentropic flow of Fig. 4d, with an associated reduction in slenderness, but also in aerodynamic efficiency. Clearly there is a compromise to be achieved between aerodynamic efficiency (assessed in the light of shock-wave losses and of the effects of chord length on skin friction and boundary-layer behaviour) and structural feasibility (in terms of slenderness and leading-edge sharpness).

Consider for example, the single-shock body, corresponding to the Nonweiler wing. In Fig. 20a, on axes showing free-stream Mach number and stagnation pressure ratio (i.e. the pressure recovery and hence, as shown, the component of Mach number normal to the wave), the shock detachment boundary shows the operating limit beyond which design flow conditions would be unobtainable.

Between this detachment boundary and the line, $M_{\text{comp}} = 1$, lies a narrow operating band in which bodies would produce attached strong oblique shock waves and subsonic discharge flows; except for free-stream Mach numbers near 1, pressure recoveries would be very poor but, at higher free-stream Mach numbers, reasonable pressure recoveries can be obtained with supersonic discharge flows. At a given free-stream Mach number, the efficiency will rise as the shock is weakened, that is, pressure recovery can be progressively improved by increasing the lateral slenderness (and M_{comp}) until at $M_N = 1$, the trivial case $M_{\text{comp}} = M_\infty$, and unit pressure recovery is reached with zero shock strength (the slenderness value is then equal to that of an isentropic body, for this free-stream Mach number and for any value of M_{comp} up to that at the turning limit of Section 4.2).

For some applications aerodynamic merit is better quoted as a kinetic energy efficiency* (*see* footnote). Lines of constant η_{KE} are shown in Fig. 20a. Each is in fact calculable as a function of pressure recovery, free-stream Mach number and γ (taken as 1·4 in this paper), so that on the axes of Fig. 20a their positions are independent of the number of shock waves produced by the body. Thus these axes and this fixed pattern of efficiency lines form a suitable framework against which variation of other features may be studied.

For bodies producing twin and triple shock waves, charts are shown in Figs. 20b and 20c; the additional scales of 'stagnation-pressure ratio per wave' show the square roots and cube roots respectively of nett values of pressure recovery. Again since any n-wave Oswatitsch system is characterised by a particular value of M_N throughout the flow, the occurrence of shock detachment will first appear with that wave having the lowest inflow Mach number, and since the flow decelerates throughout compression, this must clearly be the final wave. Detachment boundaries corresponding to this condition become rather more restrictive as n increases (*see* Figs. 20b and 20c); however, detachment is irrelevant for any system of which good efficiency is required particularly since at most Mach numbers, the external compression limit of Section 4.2 is much more restrictive and, for the triple-shock system and Mach numbers below 10, sets minimum allowable kinetic energy efficiencies of between 0·97 and 0·98. Thus while n-wave systems allow an increase in aerodynamic efficiency, related bodies are restricted to operation at these rather high levels of efficiency.

The relative significance of detachment and compression limits can, however, vary according to the application considered. For example, efficient intakes will normally require multi-shock systems, and it is worth noting that the charts originally derived for bodies such as those of Fig. 19 can be equally well used for systems as in Fig. 20d; thus for example, the chart of Fig. 20c may be used for an intake designed to produce external compression by twin shock waves and, reflected from a cowl at their focal point, a third equal shock wave, to which the detachment boundary, but no longer the compression limit, will refer.

5. *Applications.*

Various forms of caret body may be of use either as wings or in propulsive applications. For caret bodies to be used as wings, the relevance of multi-shock and isentropic bodies is not known,

* Kinetic energy efficiency, $\eta_{KE} = 1 + \dfrac{2}{(\gamma-1)M_\infty^2}\left\{1 - \left(\dfrac{{}_\iota p_\infty}{{}_\iota p_{\text{comp}}}\right)^{(\gamma-1)/\gamma}\right\}$, i.e. for an intake, the ratio of (1) the kinetic energy per unit mass flow which would be achieved by isentropic expansion of the compressed flow back to ambient (i.e. free-stream static) pressure, to (2) the kinetic energy per unit mass flow in the free stream.

and in a proposed application they would have to be compared with optimised forms of the single-shock wing. Here it is worth noting (from Fig. 21) that to obtain a high lift/drag ratio from the undersurface of a single-shock wing then, even in non-viscous flow, the wing should be operated at lift coefficients of less than 0·1; in viscous flow, low values of lift coefficient (and so of flow deflection through the single shock wave) will of course increase the influence of viscous drag compared with wave drag, but unpublished data (due to Catherall) suggests that even with allowance for the viscous drag of the laminar boundary layers expected on caret wings at high supersonic speeds, good values of lift/drag ratio may still be obtainable. In fact a variety of factors still requires consideration, for example the drags due to leading-edge bluntness, base flows and various upper surfaces, and effects of the variation of structure weight with lift coefficient and wing loading; however, if a low lift coefficient is found to be acceptable, the strength of the associated single shock wave is clearly fairly weak (*see* Fig. 21) and for wings, there may be little advantage from the use of more-complex wave systems.

For efficient engine intakes, multi-wave systems would normally be required; however, while conventional wedge intakes (with sidewalls) could be used and could be compounded with caret wings as shown by Waterhouse[13], it is unlikely that wedge intakes will produce two-dimensional flows in practice, due to flow disturbances propagated from the corners (A and B in Fig. 1c). Furthermore, wedges are structurally unfavourable in that they involve large areas which are flat or for isentropic compression of single curvature only; with caret bodies however, the use of 'curved arrowhead' planforms would clearly involve at least single curvatures, and for regions of isentropic compression, double curvatures would be required—such curvatures may be favourable structurally, and have already been shown to offer possible improvements in boundary-layer behaviour (Section 4.1). In view of these arguments for the use of caret rather than wedge intakes, some forms of caret intake are described in Section 5.1.

Since the isentropic caret body was originally derived from Prandtl-Meyer expansion wave, such bodies may be considered for use as supersonic nozzles; these and other forms of caret nozzle are described in Section 5.2.

Finally in Section 5.3, it is shown that while a variety of bodies may be designed for high individual efficiencies and for use in isolation, they are equally suitable for vehicles in which engine and airframe are to be integrated, and that resulting configurations can apparently be both aerodynamically and structurally realistic. It is considered that this easy compatibility between bodies designed as described in this paper, forms one of the major arguments in their favour.

5.1. *Intakes.*

Any caret body (or wedge with sidewalls) which produces two-dimensional compression through multi-shock or shock-plus-isentropic flow systems, can be operated at design conditions at two free-stream Mach numbers, simply by adjustment of the incidence (*see* Fig. 22a); if fitted with a cowl for use as an intake, a typical body might produce the flows shown in Fig. 22b. Clearly, at the lower design Mach number, the reduced mass flow (i.e. the reduced capture area) must be compatible with propulsion requirements; but the variation in capture area with free-stream Mach number is seen to occur at least in the right sense.

For the flow of Fig. 22b, possible intakes are shown in Fig. 22c; in comparison with those using fully internal compression, such intakes appear to offer

(1) the availability of two design Mach numbers without complex variable geometry,

(2) potential availability of trim forces from the intake loads,

(3) reduced aerodynamic sensitivity to incidence changes at a given flight Mach number, particularly since adjustment of intake incidence is assumed available for (1) above,

(4) at least partial elimination of flow disturbances due to the presence of corners, and

(5) a large measure of external compression which should ease intake starting and control, and possibly the problem of cooling.

However, for an intake having for example, inverted-V anhedral and producing a certain flow model at the design free-stream Mach number, there is an infinite choice of anhedral angle, provided that $(\frac{1}{2}z_{\text{focus}}\ 2s =)sz_{\text{focus}}$, i.e. the capture area, is kept constant at that required by the propulsion system. Thus as anhedral angle is increased, z_{focus} must increase and (for the required flow model), so must the root-chord length. Members of a family of bodies of constant capture area could therefore be as in Fig. 23; if all bodies have streamwise upper surfaces, these will be tangential to a particular 'family hyperbola', defined by the chosen value of (sz_{focus}).

Now for the spanwise station corresponding to a particular local value of root Mach number, each body will have a different value of spanwise arc length across the compression surface, and so for that particular value of nett pressure rise at the root, different spanwise pressure gradients will be produced by different bodies*. Even for simple inverted-V anhedral, the choice of angle at a constant capture area is therefore more complex than in the case of constant z_{focus} illustrated in Figs. 11 and 12, and for instance, boundary-layer considerations are further complicated by associated variations in body length and so of adverse chordwise pressure gradients, of structure weight and, due to variations in wetted area, variations of skin friction. For anhedral forms leading to 'curved arrowhead' or fully rounded planforms, the spanwise curvatures of the compression-surface body sections are much more pronounced (*see* Fig. 14), and the problem of anhedral selection is complicated even further.

If however, anhedral is finally chosen so that, as with the intakes of Fig. 22c, a rather wide cowl is required, then if the latter is inclined slightly to the free stream, it may experience a significant lift force; thus, to avoid loss of lift due to this flow spilling sideways, structural containment of the cowl pressure field might be desirable. In fact, configurations based on this principle can be compounded from bodies derived from the Nonweiler wing, but it will be shown that such methods of integration can also be extended to nozzles and exhaust flows. Various forms of nozzle are now described.

5.2. *Nozzles.*

While Prandtl-Meyer nozzles can clearly be designed in caret form, the requirement for the conventional nozzle lip will clearly involve a base drag and perhaps flow separation as in Fig. 24a. For elimination of these effects, the 'half-open' nozzle has been proposed (*see* Fig. 24b), and while such a flow could be provided by a rectangular nozzle with sidewalls, it is clear that structural walls could equally well be located along chosen streamline pairs (for example A and B in Fig. 24b); it follows that half-open nozzles providing isentropic, two-dimensional expansion may be designed to produce discharge flows of virtually any desired cross-section. Clearly, for zero base drag, the

* Note that if, in a defined family of inverted-V bodies, spanwise pressure gradients are to be maximised across a particular station, then for the case when skin curvatures are negligible, the local anhedral angle must be 45° (*see* Appendix I).

only acceptable streamline for the shorter of any pair is S_L, since this alone is of zero curvature; nozzles of this type would therefore have lips as shown in Fig. 24c, whereas swept lips are obtainable (*see* inset) only by reintroducing some base area.

For a full-scale air-breathing propulsion system operating at a high Mach number, full expansion of the nozzle flow normally requires a very large area ratio and further, the area required for the nozzle exit may be several times as large as that for the intake; to avoid the very large nozzles implied by such conditions, exit flows are frequently 'under-expanded'. In the flow of Fig. 24b, this would require the uniform external flow to be of lower static pressure than that of the nozzle flow across the final characteristic C; an additional (Prandtl-Meyer) expansion E would then form (*see* Fig. 24d), and for equal pressures and flow directions on either side of the shear layer L, an additional plane shock, S, or continuous compression wave, F. Either nozzle can thus produce two-dimensional (internal) expansion, together with a two-dimensional interaction with a uniform external flow.

The provision of a 'back pressure' by this flow interaction of course reduces the required expansion ratio of the nozzle, and so, for a given throat size and mass flow, the nozzle length and exit depth; however, this 'back pressure' could as well be produced by a plane shock wave formed not by under-expansion but for example, by the presence upstream of a caret wing. Relative to the prevailing 'back pressure' the nozzle flow could then be locally fully expanded, and so, as in Fig. 24b, would be discharged parallel to the lifting flow. With or without local under-expansion, it is evident that

(1) the implied downward deflection of a nozzle discharging for example into the flow beneath a caret wing is fully compatible with the principle of deriving lift from the propulsive flow of hypersonic vehicles, and that

(2) with the proviso that some form of structural containment is probably required for these exhaust flows, the provision of a back pressure should allow the actual nozzle to be shorter (and hence lighter) in comparison with that providing full expansion to ambient conditions.

Clearly however, the practical importance of such nozzles and exhaust flows, and the manner in which they should be operated under full-scale conditions, must depend in part upon the ease with which they may be integrated into adequate and realistic configurations. The next section contains a brief demonstration of configurations which, at design conditions, achieve fully two-dimensional integration of the intake, wing and nozzle flows beneath their lower surfaces.

5.3. *The Design of Integrated Configurations.*

Fig. 25 shows possible flow models for hypersonic air-breathing propulsion systems which use internal heat addition and produce two-dimensional fields of flow. In Fig. 25a, the cowl shock wave is of different strength to the initial intake shock wave and the flow from the 'half-open' nozzle is locally fully expanded. In Fig. 25b, the initial shock wave FG is assumed to be propagated across the entire flow, and the discharge flow from the 'half-open' nozzle to be under-expanded; the flow interaction then produces a plane shock S as previously noted in Section 5.2, and although the losses across this shock wave could well be small, they can in principle be eliminated as in Fig. 25c. By selection of various stream surfaces from these flow models, configurations may be defined in such a way that, at design conditions and excepting those flows ducted internally (and hence excepting the heat addition processes themselves), both lifting and propulsive flows are aerodynamically two-dimensional and structurally 'contained'.

For example, in Fig. 25a, the region ABCD comprises uniform flow behind the plane shock AD, and so, with AC as a partly aerodynamic, partly structural 'lower ridge line', this flow could be regarded as that beneath a Nonweiler wing. If for simplicity, trailing edges are located upstream of the expansion E, then clearly a configuration could resemble that of Fig. 26a, in which the purely lifting flow is provided effectively by the body shown inset (the area P_1 corresponding to the shear layer in Fig. 25a).

In Fig. 25b, the flows in the regions FGHJK and downstream of GH are also uniform and together could correspond to the two-dimensional flow beneath a two-shock variant of the Nonweiler wing, having separate structural and aerodynamic 'lower ridge lines', JH and HL; a configuration to produce this flow could then be as in Fig. 26b (the purely lifting flow is again related to that of the body shown inset, and the shear layer to the area P_2). Finally if S, the shock due to under-expansion is replaced as in the flow of Fig. 24c, by an isentropic compression wave, a further configuration results (*see* Fig. 25c).

Basically, the above method comprises two steps:

(1) the design of an appropriately integrated two-dimensional, aero- and thermodynamic flow model, and assessment of the required ratio of propulsive and lifting capture areas, and

(2) the definition of stream surfaces within this flow model, with which structural walls may be realistically aligned, and of which the aerodynamic stability and control may be regarded as acceptable.

In full-scale applications, flow geometry will depend upon flight Mach number and intake efficiency and the degree of under-expansion in the nozzle flow, and these in turn upon operational objectives; thus, the above examples show only that in principle, bodies previously derived from the Nonweiler wing can be compounded in configurations which are probably realistic structurally, and which while integrating the aero- and thermodynamic flow fields, retain the two-dimensional nature of the component flows.

6. *Proposed Experimental Work.*

Models already tested or existing are listed in Table 1. For comparison, pairs of variant bodies producing respectively twin-shock and shock-plus-isentropic, centred compression have been designed for operation at the same combinations of free-stream and discharge Mach number. By reference to Table 2 and Figs. 27a and 27b (for Models A and B) and Figs. 27c and 27d (for Models D and C), it will be seen that, for the second of each variant pair, the rear shock wave is replaced by an isentropic wave producing the same change in Mach number but ideally with zero loss in stagnation pressure.

Of the existing models, it is seen from Table 1 that, in relation to their design Mach numbers, Models A, D, 2 and 5 all produce moderately good shock efficiencies and so, as shown in Table 2, benefit little by modification to centred compression. So, for free-stream Mach numbers of 6·85 and 4·30, only Models B_2, B_{1+}, C_2 and C_{1+} should be made initially; however, since values of pressure ratio across the isentropic wave (*see* Table 2) may be high enough to force separation on the curved surfaces of at least one of Models B_{1+} and C_{1+}, these should allow for boundary-layer removal or for easy conversion to cropped caret configurations—failing this, it might be necessary to construct Model D_{1+} and perhaps for comparison, Model D_2. Appropriate measurements would be of the effects of incidence upon the pressure distributions at various stations and since conical

flow would not be maintained at off-design conditions, of aerodynamic forces also; other observations could be usefully made of oil-flow patterns on the surface (especially in the region of ridge lines and compression corners), of shock and wake flow structures, and of shock-wave detachment at incidence and the effects of yaw.

Model E is also to be tested in an existing programme at the design Mach number of 2·47. It is unlikely that at this low Mach number, caret bodies are suitable as wings, but it is seen from Fig. 20a and Table 1 that while efficiency is good, the value of discharge Mach number (1·97) is so high that this body would not be used as an intake except with further supersonic diffusion. The addition of a second (equal) shock wave is impracticable since for this value of M_N (1·39), it would be detached; consequently no variant of Model E (or of Model G) is proposed for test.

For tests on bodies with inverted-U anhedral forms, it seems likely that some initial studies of oil flows, and probably a few tests of the pressure fields on models in flows of Mach numbers up to 5 could usefully be conducted. Of course, even initial tests should cover the effects on boundary-layer transition and separation of parameters such as free-stream Mach number, Reynolds number and the degree of compression, and anhedral and planform design; thus, a rather large number of models would be required and, at least for tests at design conditions, each would be of rather limited utility. Furthermore, it seems likely that results obtained with early models should in part dictate later tests, so that new models should be rapid and cheap to manufacture. On the results of such tests and of supporting analytic studies, a few larger models could be designed for much more exhaustive flow traversing and pressure plotting, preferably in continuous flows of high Mach number and at high stagnation pressure and temperature.

The various sources of difficulty in such a programme are evident, but must be assessed against the convenience of studying three-dimensional boundary layers with external flows which are two-dimensional, and which impose pressure fields which can be closely defined.

Another model which might involve surfaces having double-curvature would be that of a 'half-open' nozzle, resembling for example those of Fig. 24c. Experimental data would in fact be additional to those from tests which are about to begin on a conventional 'half-open' nozzle (i.e. a profiled wedge with sidewalls), in which tests the free-stream and design nozzle exit Mach numbers are to be 4·3 and 3 respectively. With this existing wind-tunnel installation it is possible to produce a considerable degree of under-expansion, and results for nozzles of conventional and caret form would thus allow comparison both at design conditions and those of Fig. 24d.

7. *Conclusions.*

Design principles have been described for bodies which have various forms of anhedral and which, at design combinations of Mach number and incidence, 'contain' between their lower surfaces, multi-shock or isentropic, centred compression waves. As with the Nonweiler wing, a complete compression surface can be designed if the capture flow tube and the required two-dimensional flow model are defined; in this report, all wave systems have been chosen to satisfy the Oswatitsch condition for maximum pressure recovery, and this is shown to govern the shapes of related bodies.

Bodies producing centred compression have

(1) the focal line of the compression wave passing through the tips,

(2) streamwise body sections that are geometrically similar and correspond to particular streamlines in the relevant two-dimensional flow model,

(3) leading and trailing edges which are aligned in the planes of the chosen initial and discharge compression waves, a condition which, for isentropic bodies, will normally impose pointed or rounded 'arrowhead' planforms; further,

(4) for a particular body, the planform and anhedral distribution, the capture flow tube and all waves in the compression are isomorphic (i.e. all triangular, all parabolic, etc.)—however, with added regions of uniform flow, planforms can be considerably modified, and may for example, be altered from arrowhead to delta planform.

For isentropic bodies, changes in planform and so in anhedral distribution dictate changes in spanwise pressure distributions, and consideration of boundary-layer conditions suggests that anhedral should increase towards the body tips, which implies the need for 'curved arrowhead' planforms (as in Fig. 14); if the corner flow along the lower ridge line is also to be eliminated, leading and trailing edges will form continuous curves from tip to tip. For any planform, pressure gradients at the extreme tips may require special attention since, with multi-shock or isentropic systems, the occurrence of large pressure gradients and also of shock waves may induce boundary-layer separation.

Bodies derived from two-dimensional flows have been shown to be applicable both as intakes and nozzles; further, by extension of the design principle to complete propulsive flow models, realistic configurations can be designed for aircraft, beneath which the lifting and propulsive flows are fully integrated and, at design conditions, wholly two-dimensional.

For wind-tunnel tests, models have been proposed in three forms: firstly, as inverted-V bodies producing compression by means of twin-shock or single-shock-plus-isentropic wave systems and intended for investigating the variation of forces and pressure distributions with incidence: secondly for boundary-layer research, they are proposed in purely isentropic form, with anhedral distributions designed to impose certain spanwise pressure distributions across the compression surfaces: thirdly, a 'half-open' nozzle, designed as described in this paper, could provide results for comparison with those from an existing model of conventional form (i.e. profiled wedge plus sidewalls).

In addition, a study could be made of the following:

(1) the effects on body shape of γ-variation due to rises in static temperature as compression proceeds,

(2) the need for boundary-layer removal and possible effects on performance of related drag forces,

(3) the possibility of optimising anhedral distributions (and so planform design) in the light of (a) boundary-layer behaviour, (b) skin friction or wetted area per effective lifting area, and (c) available enclosed volume, and

(4) in the light of the above, the relative merits in applied forms of various single-shock, multi-shock or isentropic bodies, and comparison of these with other types of lifting body.

LIST OF SYMBOLS

c	Chord length
C_L	Lift coefficient
D	Drag force
l	*See* Fig. 23
l_1, l_2	*See* Fig. 13c
L	Lift force
m	See Fig. 23 and Appendix
M	Mach number
n	Number of shock waves in multi-shock system
p	Static pressure
${}_\iota p$	Stagnation pressure
r	See Fig. 7
s	Semi-span
S	Planform area
x, y, z	Lengths measured parallel to the conventional orthogonal axes (*see* Figs. 13 and 23)
γ	Ratio of specific heats for air (taken as 1·4)
δ	Angle of flow deflection through a shock wave
ζ	Shock-wave angle relative to free-stream direction
η_{KE}	Kinetic energy efficiency of supersonic air intake
ϕ	See Fig. 7
μ	Mach angle $\left(= \sin^{-1}\frac{1}{M}\right.$, for a uniform flow of Mach number $\left.M\right)$
ν	Prandtl-Meyer flow angle (*see* Fig. 4a)

Suffices

∞	. . . of the undisturbed free stream
comp	. . . of the compressed flow
exp	. . . of the expanded flow
focus	. . . referred to the focal point of the compression wave(s)
N	normal component of . . .
root	. . . of the root section

REFERENCES

No.	*Author(s)*	*Title, etc.*
1	D. Küchemann	On some three-dimensional flow phenomena of the transonic type. Proceedings of the I.U.T.A.M. Symposium Transsonicum, Aachen, 1962. Springer-Verlag, Berlin. 1964.
2	G. I. Maikapar	On the wave drag of axisymmetric bodies at supersonic speeds. Russian J. App. Math. Mech. (Pergamon translation), Vol. 23, No. 2, pp. 528 to 531. 1959.
3	T. R. F. Nonweiler	Aerodynamic problems of manned space vehicles. *J. R. Ae. Soc.*, Vol. 63, No. 585, pp. 521 to 528. September, 1959.
4	T. R. F. Nonweiler	Delta wings of shapes amenable to exact shock-wave theory. A.R.C. 22,644. March, 1961. Also *J. R. Ae. Soc.*, Vol. 67, No. 625, pp. 39 to 40. January, 1963.
5	L. C. Squire	Some notes on wings of inverted-V cross-section. Unpublished M.O.A. Report.
6	D. Peckham	On three-dimensional bodies of delta planform which can support plane attached shock waves. A.R.C. C.P. 640. March, 1962.
7	J. A. Bagley	An estimate of the lateral forces and moments on yawed caret wings. A.R.C. 24 057. April, 1962.
8	D. Catherall	Boundary layer characteristics of caret wings. A.R.C. C.P. 694. May, 1963.
9	L. C. Squire	Pressure distributions and flow patterns at $M = 4{\cdot}0$ on some delta wings. Part I. Wing of inverted-V cross-section. A.R.C. R. & M. 3373. February, 1963.
10	L. Pennelegion and R. F. Cash ..	Preliminary measurements in a shock tunnel of shock angle and undersurface pressure related to a Nonweiler wing. A.R.C. C.P. 684. July, 1962.
11	D. M. Sykes	Flow visualisation studies of plane and caret delta wings at supersonic and hypersonic Mach numbers. Royal Armament Research and Development Establishment R.A.R.D.E. Memo (B) 59/62. December, 1962.
12	D. Treadgold	Pressure distributions at $M = 4{\cdot}3$ on some delta wings of inverted 'V' cross-section with various angles of sideslip. Unpublished M.o.A. Report.
13	J. F. Waterhouse	π-bodies—further notes on a class of shock interference designs. Unpublished Note, Whitworth-Gloster Aircraft Limited. July, 1962.

REFERENCES—*continued*

No.	*Author(s)*	*Title, etc.*
14	K. Oswatitsch	Pressure recovery for missiles with reaction propulsion at high supersonic speeds. (The efficiency of shock diffusers.) N.A.C.A. Tech. Memo. 1140. June, 1947.
15	J. W. Flower	Configurations for high supersonic speeds derived from simple shock-waves and expansions. *J. R. Ae. Soc.*, Vol. 67, No. 629, pp. 287 to 290. May, 1963.
16	A. C. Southgate and J. R. Pedersen ..	Comment on 'Delta wings of shapes amenable to exact shock-wave theory'. *J. R. Ae. Soc.*, Vol. 67, No. 629, p. 301. May, 1963.
17	J. G. Jones	A method for designing lifting configurations for high supersonic speeds using the flow fields of non-lifting cones. A.R.C. 24 846. March, 1963.
18	B. A. Woods	The construction of a compression surface based on an axisymmetrical conical flow field. A.R.C. 25 087. June, 1963.
19	E. C. Maskell and J. Weber	On the aerodynamic design of slender wings. *J. R. Ae. Soc.*, Vol. 63, No. 588, pp. 709 to 721. December, 1959.
20	G. S. Raetz	A method of calculating three-dimensional laminar boundary layers of steady compressible flows. Northrop Aircraft Inc., Report NAI–58–73(BLC–114). December, 1957. A.R.C. 23 634. March, 1962.
21	J. C. Cooke and M. G. Hall	Boundary layers in three-dimensions. *Progress in Aeronautical Sciences*, Vol. 2. Pergamon Press. 1962.
22	J. F. Connors, R. R. Woollett and R. E. Blue.	Interferometric observation of flow about an isentropic (reverse Prandtl-Meyer streamline) compression wedge at Mach 3·0. N.A.C.A. Research Memo. E55A28. March, 1955.
23	N. H. Johannesen	Experiments on two-dimensional supersonic flow in corners and over concave surfaces. Fluid Motion Laboratory, University of Manchester. A.R.C. 14 607. January, 1952.
24	J. F. Connors and R. C. Meyer ..	Design criteria for axisymmetric and two-dimensional supersonic inlets and exits. N.A.C.A. Tech. Note 3589. January, 1956.
25	E. Eminton	Simple theoretical and experimental studies of the flow through a three-shock system in a corner. A.R.C. C.P. 727. September, 1961.

APPENDIX

Consider a family of isentropic caret bodies, every member designed for the same values of M_∞ and M_{comp}, and for the same capture area. Then, $s_1(z_{focus})_1 = s_2(z_{focus})_2 = \ldots = s_n(z_{focus})_n$, and hence the 'family hyperbola' of Fig. 23 is obtained. But $s_n(z_{focus})_n = s_n(c_{root})_n (z_{focus}/x_{focus})(x_{focus}/c_{root})$, so that since z_{focus}/x_{focus} is a function of M_∞ and x_{focus}/c_{root} of M_∞ and M_{comp}, the family condition may be restated as $s(c_{root}) = \text{const}$. Now the local semi-span at a chordwise station

$$x = m(c_{root})$$

is $y = (mc_{root}/x_{focus})s$ and corresponds for a given m, to a particular value of root Mach number (and so of static pressure above the free-stream value) for any body in the family. If skin curvature is ignored, the spanwise skin length over which the static pressure falls to the free-stream value is therefore

$$l = \sqrt{\left\{\left(\frac{mc_{root}s}{x_{focus}}\right)^2 + (mc_{root}\tan\mu_\infty - d)^2\right\}}.$$

Now if, in a given family designed for specified values of M_∞ and M_{comp}, there is one particular body on which the skin length at a defined station (i.e. a given m) becomes a minimum, then the spanwise pressure gradient at that station is maximised; if curvature effects are ignored, differentiation of the above expression gives the condition for maximum pressure gradient, from which the corresponding anhedral may be determined. For minimum skin length,

$$As^2 = \frac{B}{s^2},$$

in which expression,

$$A = \left(\frac{mc_{root}}{x_{focus}}\right)^2 = \left(\frac{y}{s}\right)^2,$$

$$B = \left(msc_{root}\tan\mu_\infty - \frac{d}{c_{root}}(sc_{root})\right)^2;$$

thus,

$$\frac{l_{min}}{y} = \sqrt{\left\{2A\left(\frac{s}{y}\right)^2\right\}} = \sqrt{\frac{2B}{y^2(s)^2}} = \sqrt{2}.$$

Thus, the anhedral at the station at which spanwise pressure gradient is to be maximised, must be 45° (usually with some error due to neglect of skin curvature).

TABLES 1 and 2

Existing Models and Equivalent Variants (*see Fig.* 27)

Design Mach number	Test Mach number	Model No. (and Ref. No.)	Design flow deflection at leading edges (degrees)	Design shock angle at leading edges (degrees)	Aspect ratio	Length (inches)	Span (inches)	Design M_{comp}-value	Design shock M_N-value	Stagnation pressure ratio (per cent)	Static pressure ratio across isentropic fan (where applic.)	Anhedral form	
6·85	6·85	A	10·15	16·68	1	5	2·5	5·12(8)	1·96(5)	73(·7)		Inverted-V	Table 1. Existing models
6·85	6·85	B	17·73	25·02	1	5	2·5	3·91(2)	2·89(5)	35(·9)			
4·30	4·30	D	8·41	19·80	1	5	2·5	3·63(1)	1·45(7)	94(·3)			
4·30	4·30	C	16·17	27·3	1	5	2·5	3·01(8)	1·97(2)	73(·4)			
4·0	4·0	2 (Ref. 9)	10	22·2(3)	4/3	30			1·5(1)	92(·7)			
4·0	4·0	5 (Ref. 9)	10	22·2(3)	2	25			1·5(1)	92(·7)			
5·0 (Model to exhibit off-design performance)	4·0	3 (Ref. 9)	10 (at $M_\infty = 5$)		4/3	30							
2·47	2·47	E	12·13	34·28	1			1·97(2)	1·39(1)	96(·0)			
2·47	2·47	G	12·13	34·28	3/2	3·33		1·97(2)	1·39(1)	96(·0)			
6·85	6·85	A_2	5·28	12·23	These values to be decided after blockage tests in appropriate wind tunnels.			5·12(8)	1·45(1)	89(·1)		Inverted-V	Table 2. Equivalent variants (those proposed for testing, marked *)
6·85	6·85	A_{1+}	5·28	12·23				5·12(8)	1·45(1)	94(·4)	2·43		
6·85	6·85	B_2 *	9·46	16·01				3·91(2)	1·88(9)	59(·6)			
6·85	6·85	B_{1+} *	9·46	16·01				3·91(2)	1·88(9)	77(·2)	5·17		
4·30	4·30	D_2	4·23	16·39				3·63(1)	1·21(3)	98(·2)			
4·30	4·30	D_{1+} (*)	4·23	16·39				3·63(1)	1·21(3)	99(·1)	1·57		
4·30	4·30	C_2 *	8·39	19·78				3·01(8)	1·45(5)	88(·9)			
4·30	4·30	C_{1+} *	8·39	19·78				3·01(8)	1·45(5)	94(·3)	2·44		

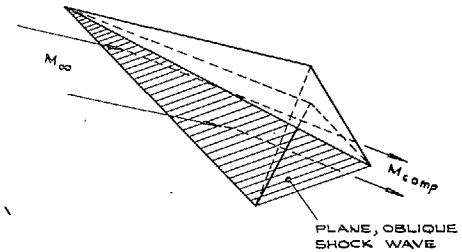

(a) SINGLE-SHOCK INVERTED-V NONWEILER WING AT DESIGN CONDITION.

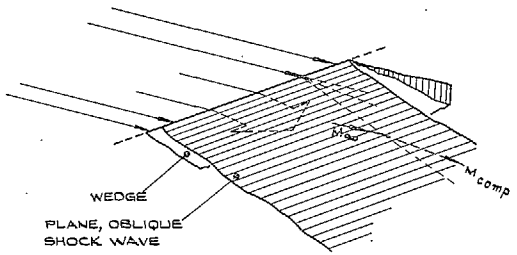

(b) INFINITE WEDGE IN UNIFORM SUPERSONIC FLOW.

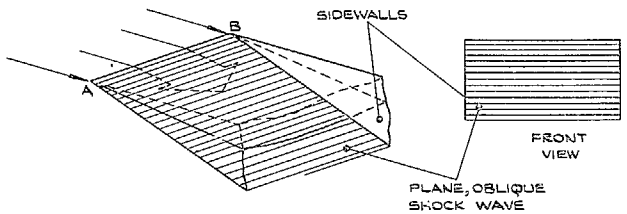

(c) SINGLE WEDGE WITH SIDEWALLS.
(TWO-DIMENSIONAL SUPERSONIC INTAKE AT DESIGN CONDITION.)

FIG. 1a to c. The inverted-V Nonweiler wing and bodies producing analogous flows.

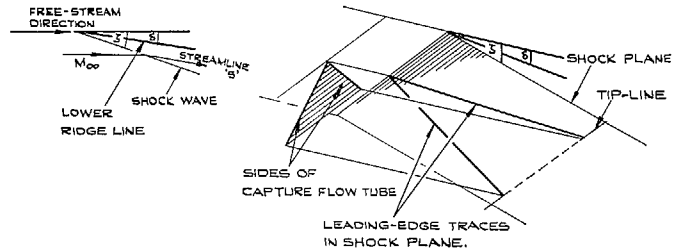

(a) FLOW MODEL. (b) FLOW MODEL, CAPTURE TUBE AND LEADING EDGES.

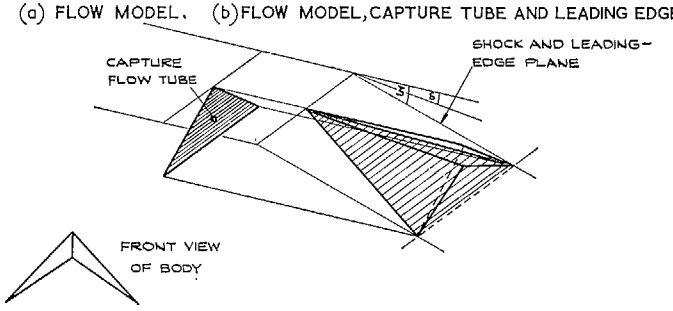

(c) CARET BODY WITH CONSTANT ANHEDRAL
(i.e. A TRIANGULAR CAPTURE FLOW TUBE).

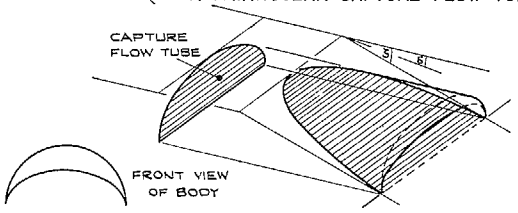

(d) CARET BODY WITH NON-UNIFORM ANHEDRAL
(HAVING A SEMI-CIRCULAR CAPTURE FLOW TUBE).

FIG. 2a to d. The effect of flow model and capture flow tube on leading-edge shape and anhedral of single-shock caret bodies.

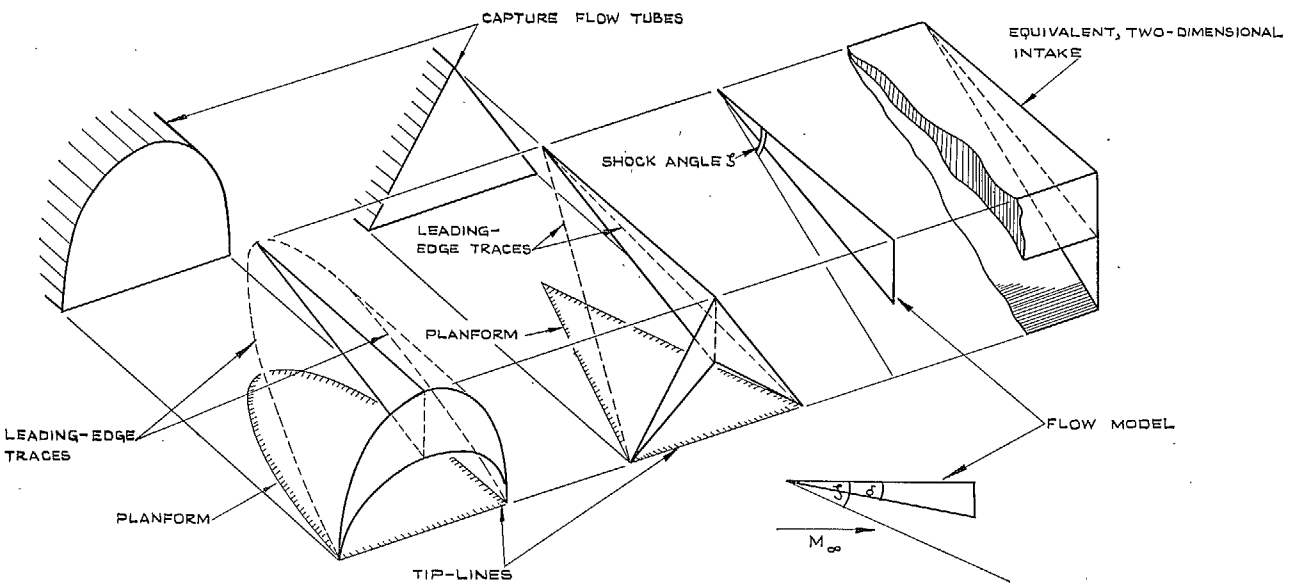

FIG. 3. Summary figure for the design of single-shock caret bodies.

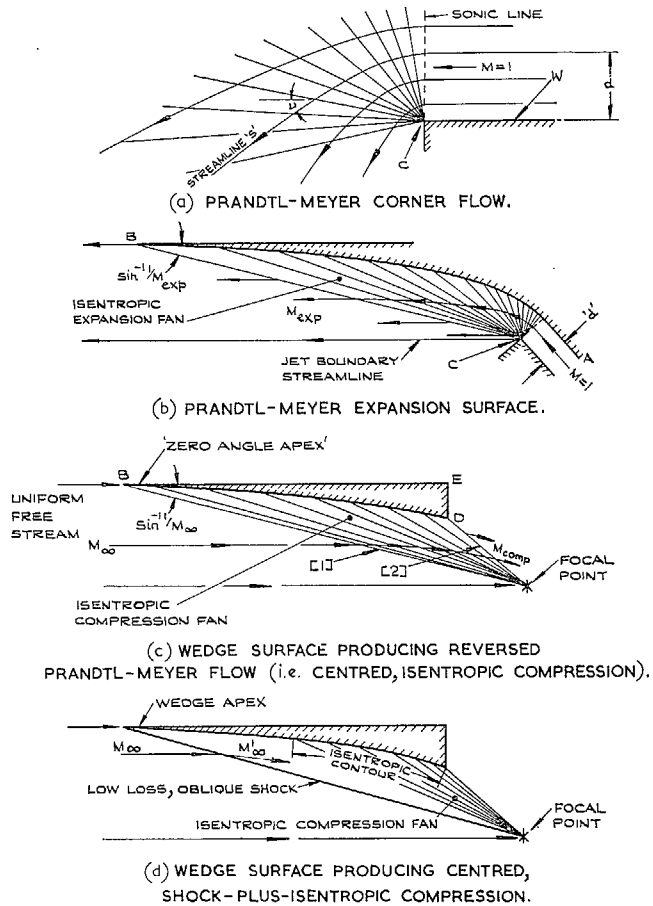

FIG. 4a to d. Two-dimensional, supersonic flows composed of centred expansion and compression waves.

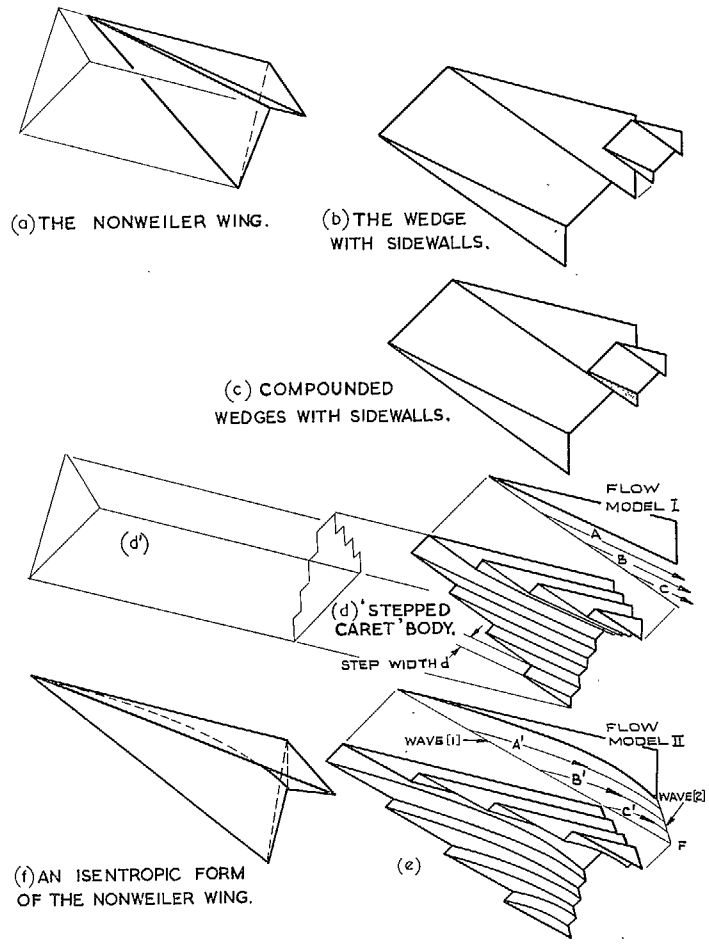

FIG. 5a to f. Derivation of an isentropic form of the Nonweiler wing.

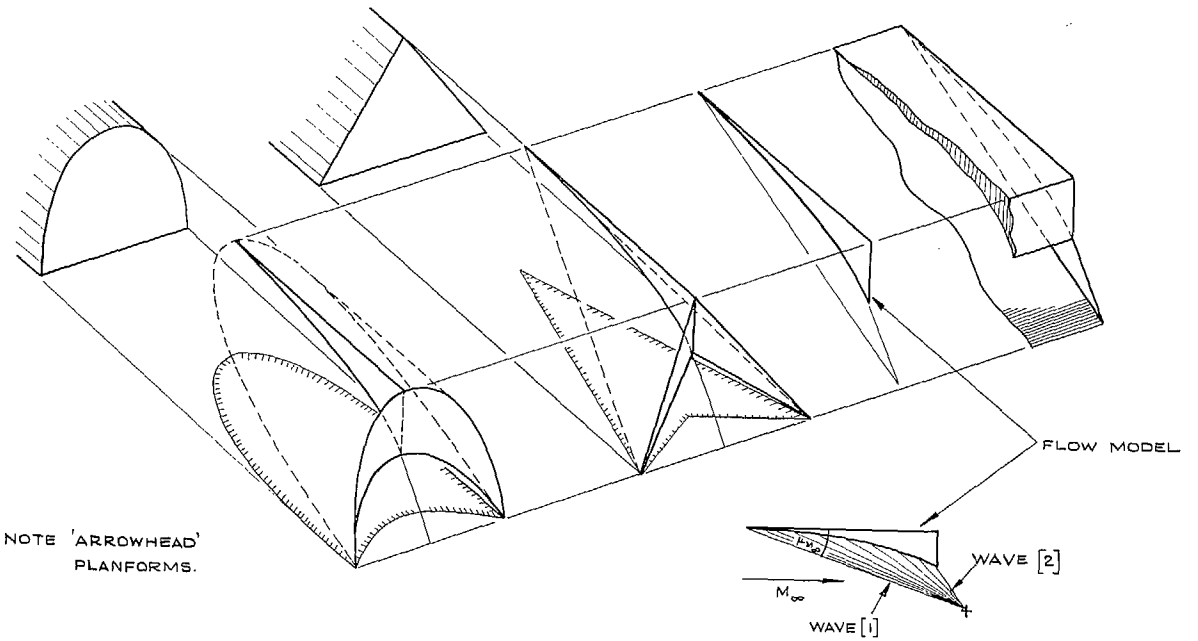

FIG. 6. Summary figure for the design of isentropic caret bodies (*see* Fig. 3).
(a) Diagram.

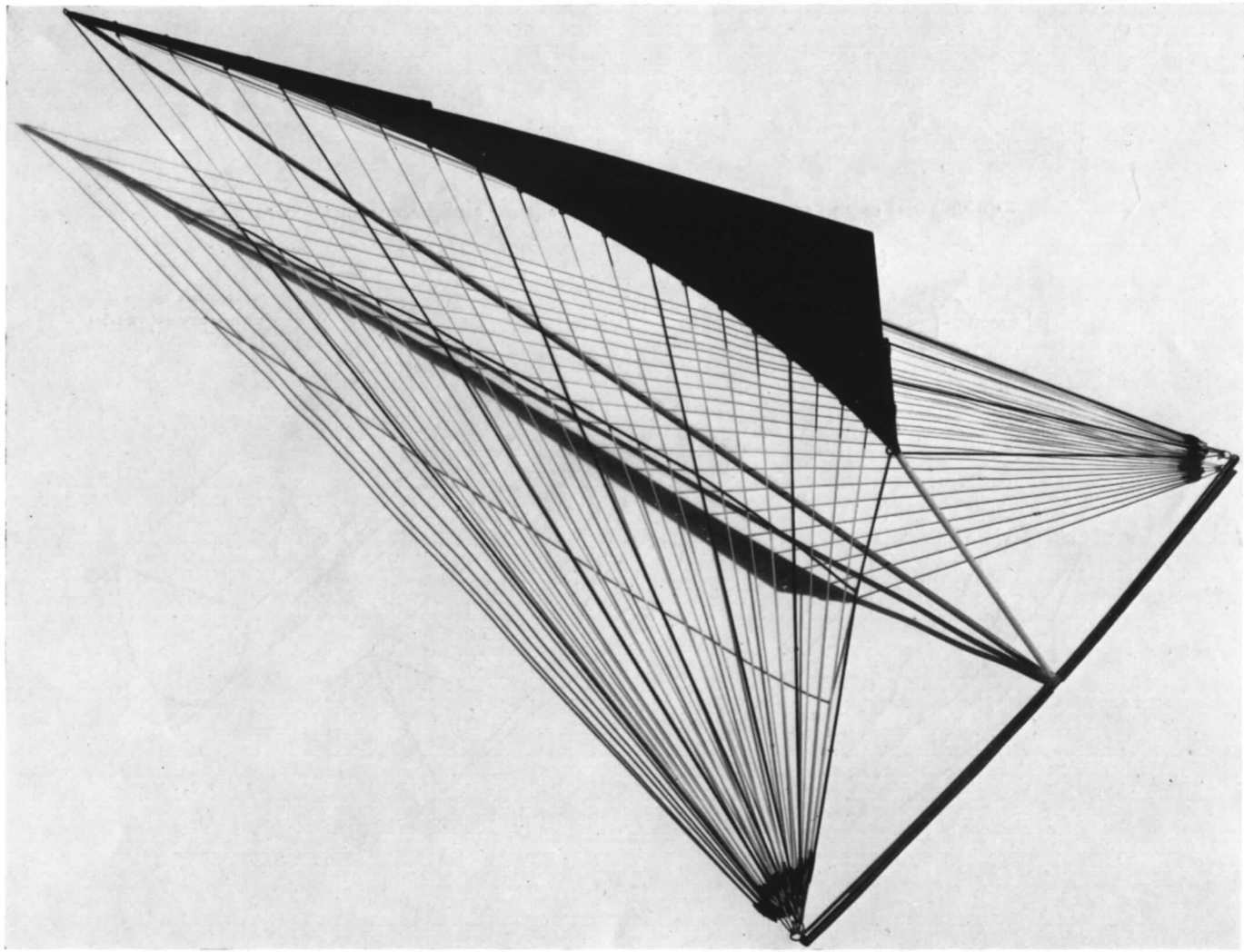

FIG. 6. Summary figure for the design of isentropic caret bodies (*see* Fig. 3).
(b) Model.

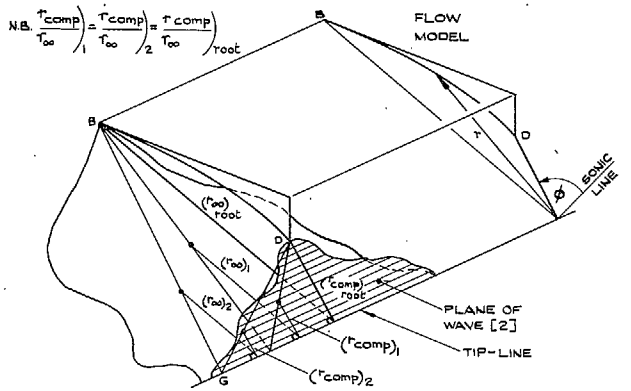

(a) LEADING- AND TRAILING-EDGE GEOMETRIES.

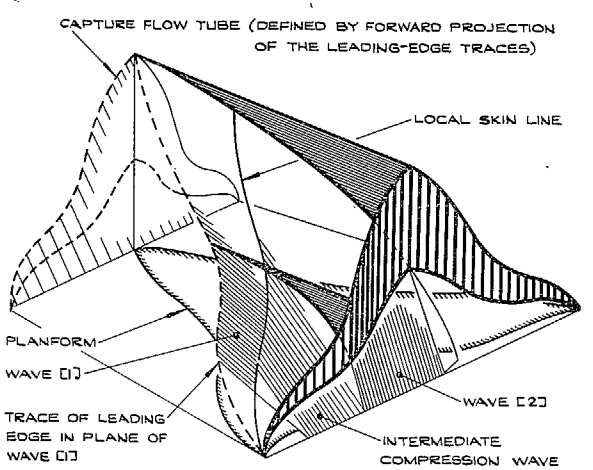

(b) COMPLETE FLOW AND BODY GEOMETRIES.

FIG. 7a and b. Isomorphic properties of a caret body.

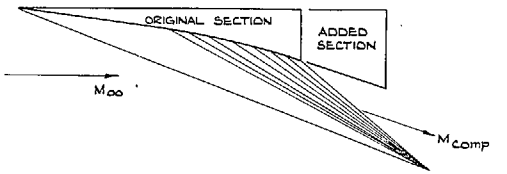

(a) MODIFIED FLOW MODEL.

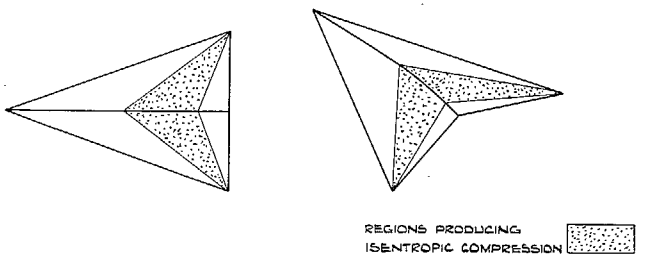

(b) DELTA PLANFORM.

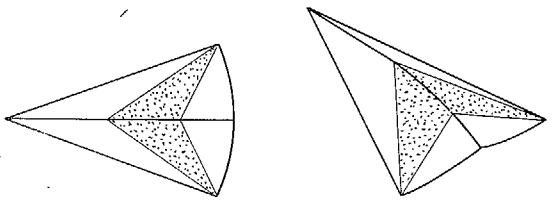

(c) CURVED-RHOMBIC PLANFORM.

FIG. 8a to c. Planform modification on bodies for a given combination of free-stream and discharge Mach number.

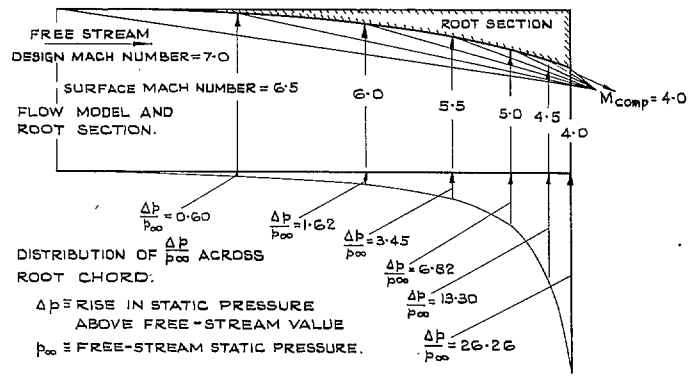

(a) FLOW MODEL AND ROOT CHORDWISE PRESSURE DISTRIBUTION.

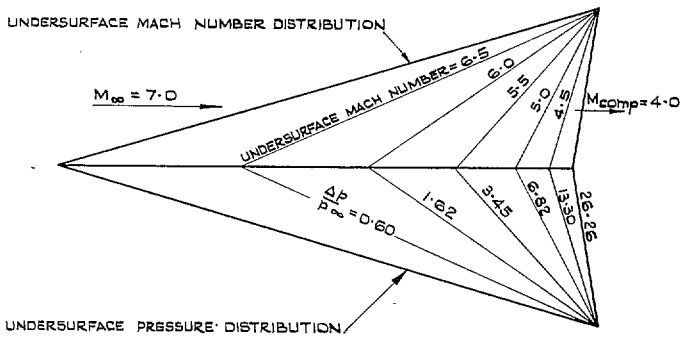

(b) ISOBARS AND UNDERSURFACE MACH NUMBER DISTRIBUTION.

FIG. 9a and b. Typical isentropic caret body designed for free-stream and discharge Mach numbers (M_∞ and M_{comp}) of 7 and 4.

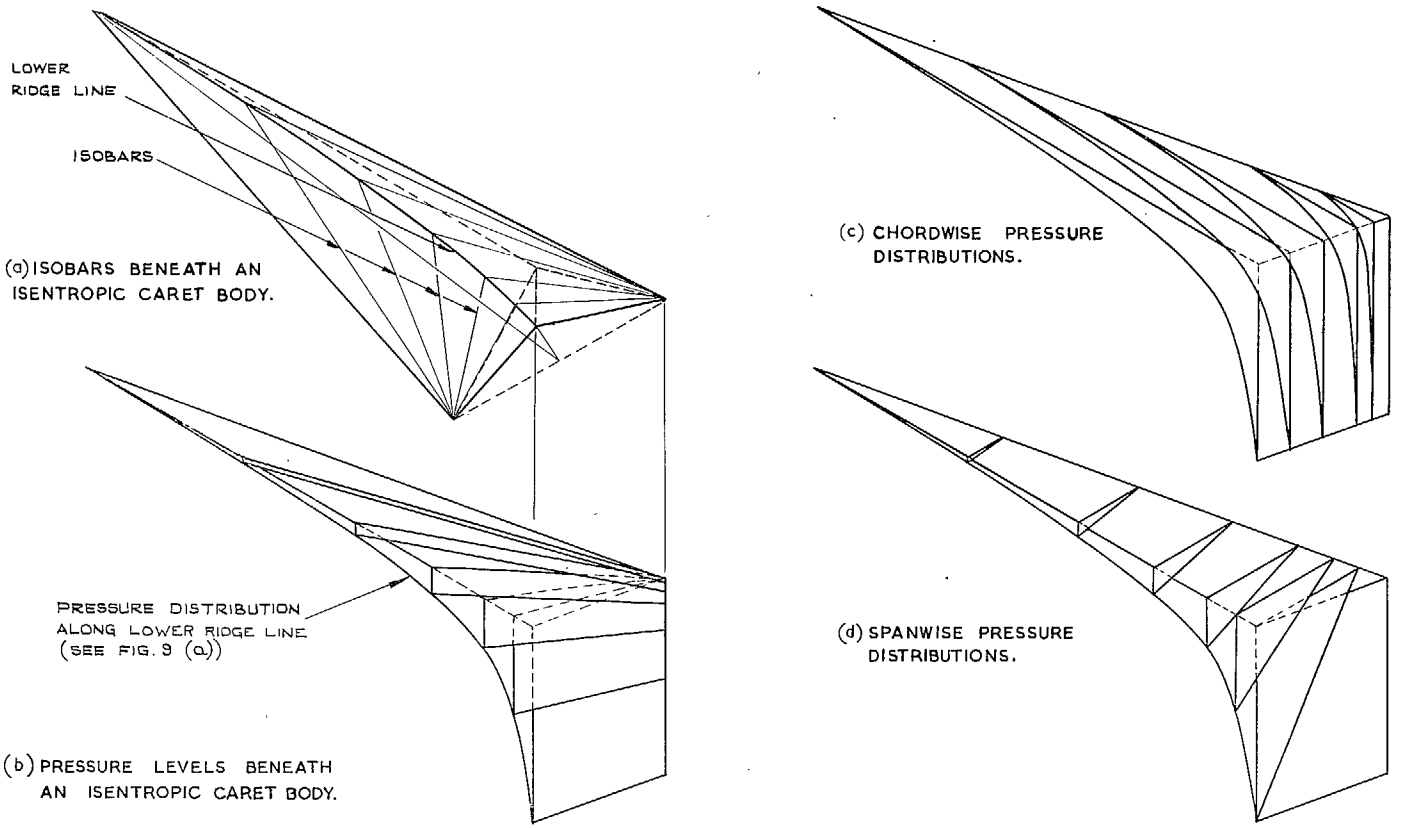

FIG. 10a to d. Pressure distributions for an inverted-V isentropic caret body designed for free-stream and discharge Mach numbers (M_∞ and M_{comp}) of 7 and 4.

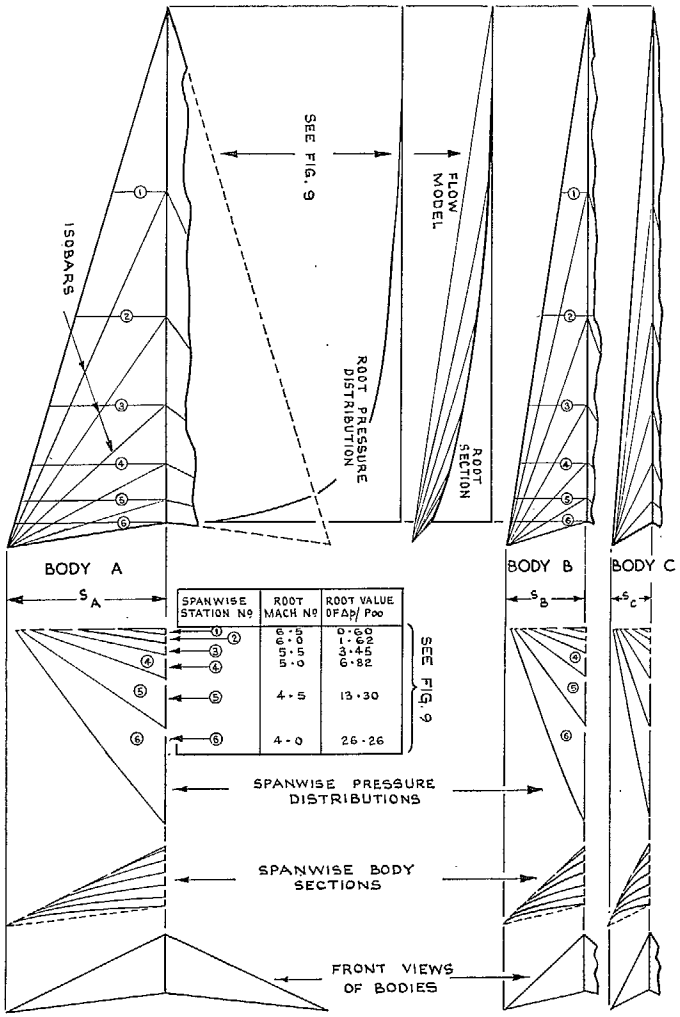

FIG. 11. Spanwise pressure distributions and body sections of three inverted-V isentropic caret bodies designed for Mach numbers (M_∞ and M_{comp}) of 7 and 4.

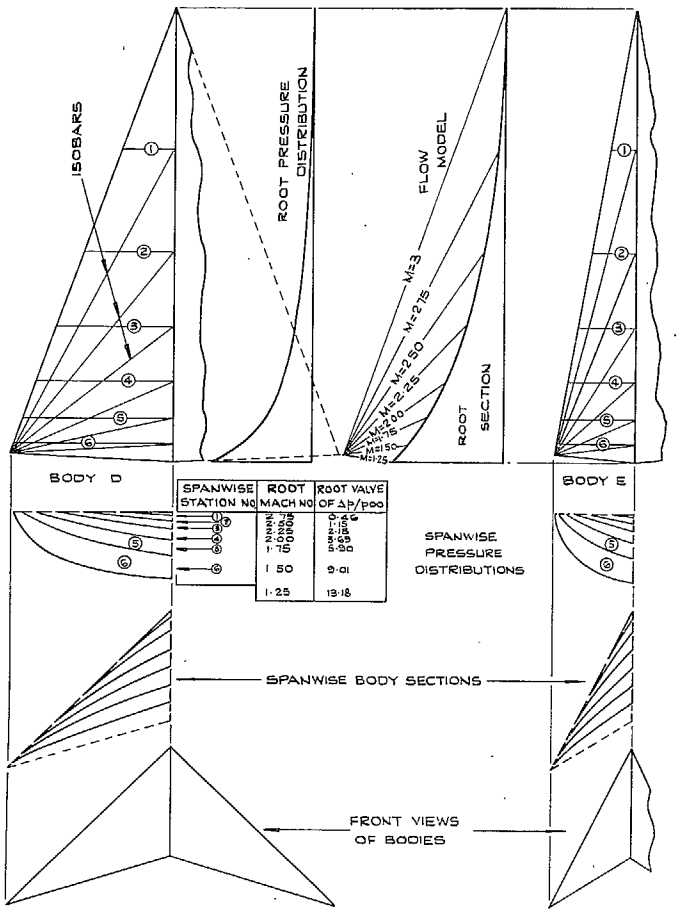

FIG. 12. Spanwise pressure distributions and body sections of two inverted-V isentropic caret bodies designed for Mach numbers (M_∞ and M_{comp}) of 3 and 1·25.

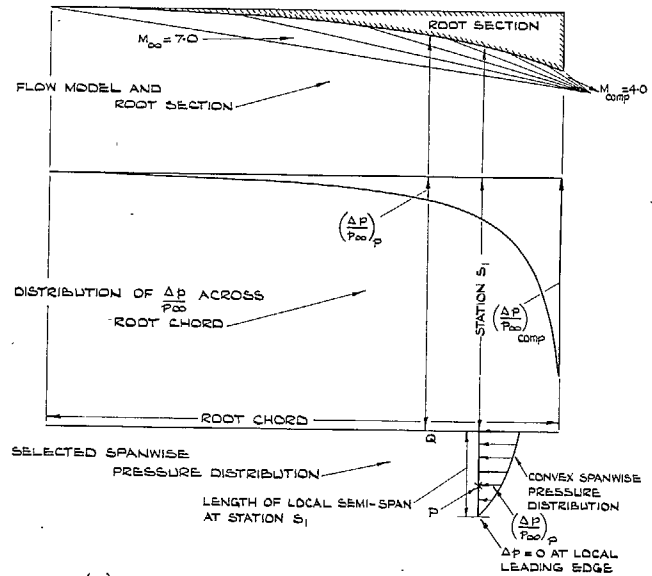

(a) FLOW MODEL AND PRESSURE DISTRIBUTIONS.

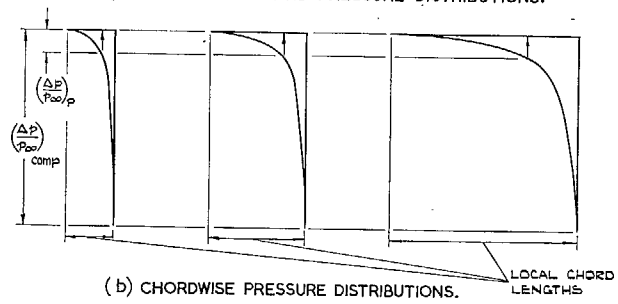

(b) CHORDWISE PRESSURE DISTRIBUTIONS.

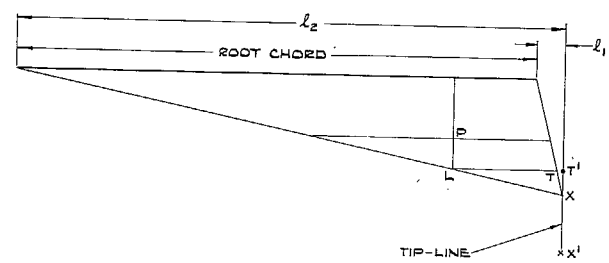

(c) LEADING- AND TRAILING-EDGE LOCATION.

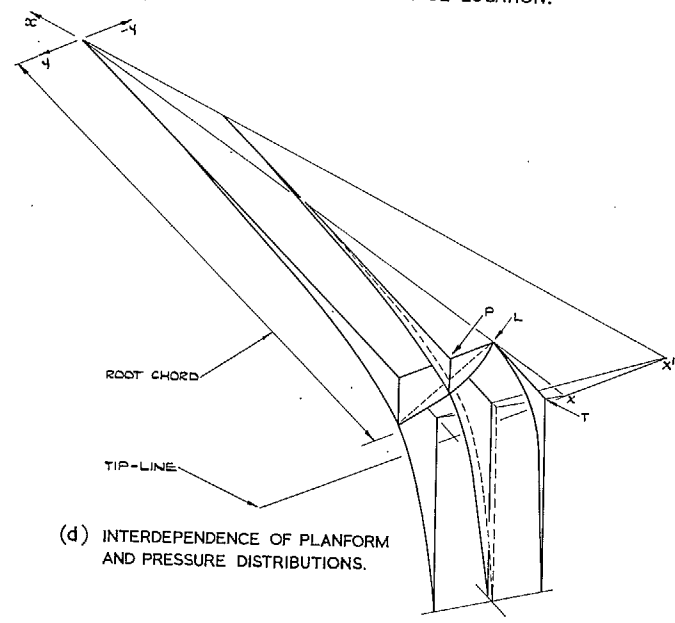

(d) INTERDEPENDENCE OF PLANFORM AND PRESSURE DISTRIBUTIONS.

FIG. 13a to d. The design of a caret body by definition of the flow model and a single spanwise pressure distribution.

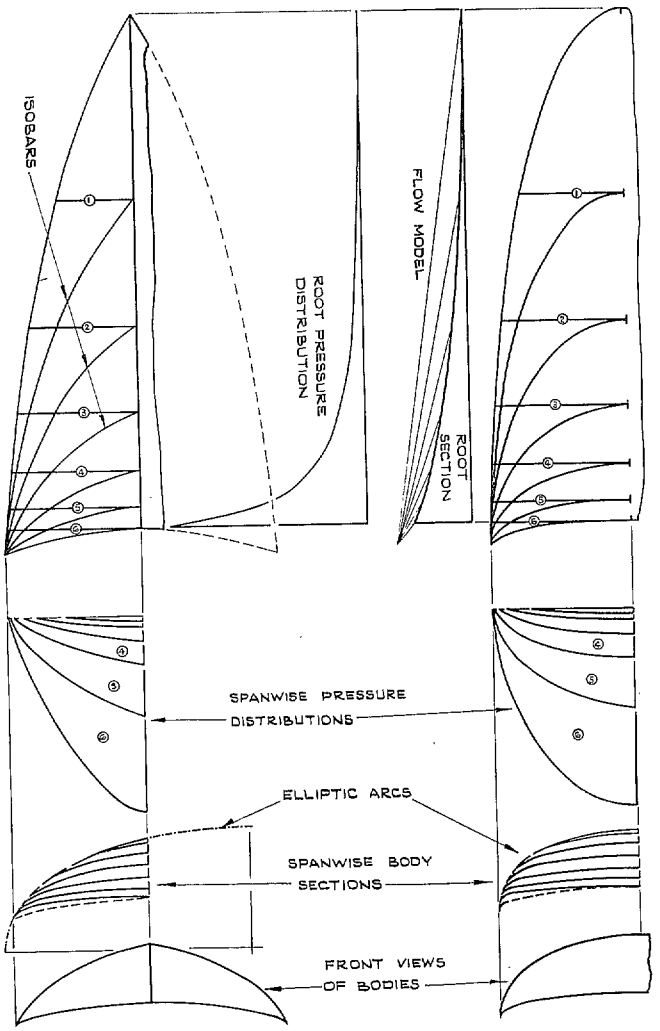

FIG. 14. Spanwise pressure distributions and body sections of isentropic caret bodies designed for Mach numbers (M_∞ and M_{comp}) of 7 and 4 (elliptically curved arrowhead planforms).

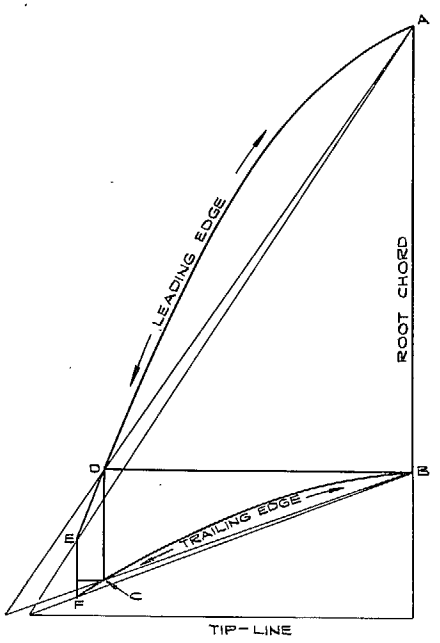

FIG. 15. Procedure for planform and tip design of isentropic caret bodies.

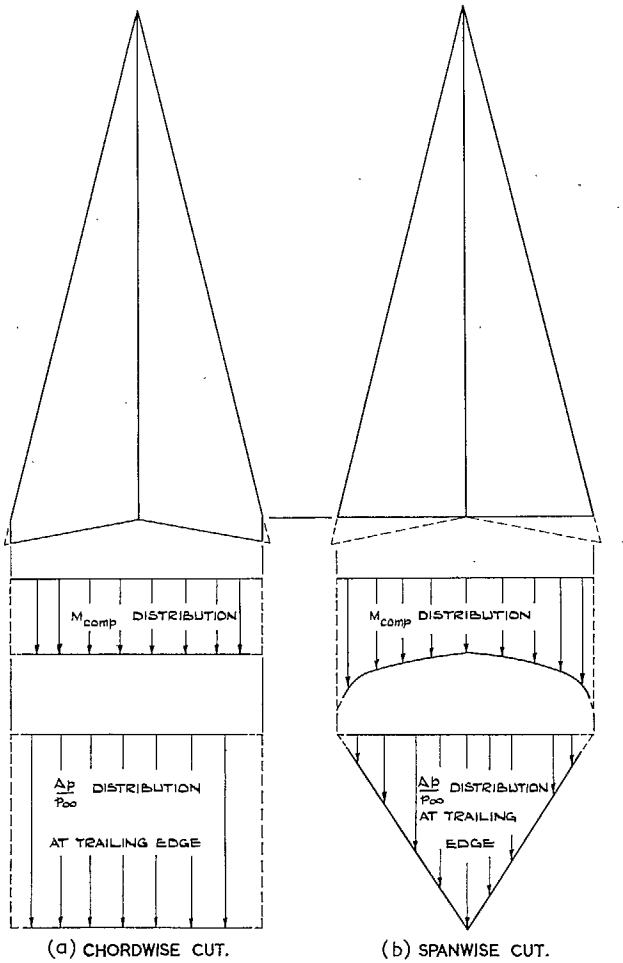

FIG. 16a and b. Possible isentropic caret bodies with cropped tips.

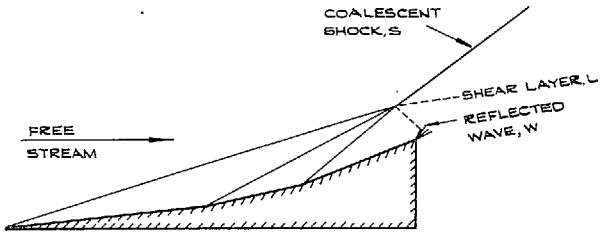

(a) n-SHOCK, CENTRED COMPRESSION.

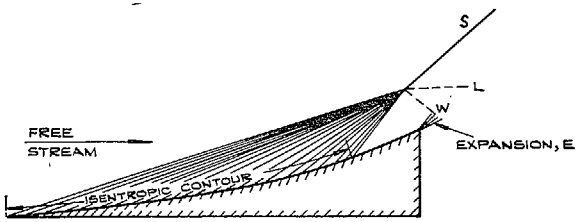

(b) ISENTROPIC, CENTRED COMPRESSION.

FIG. 17a and b. Wave systems for centred compression.

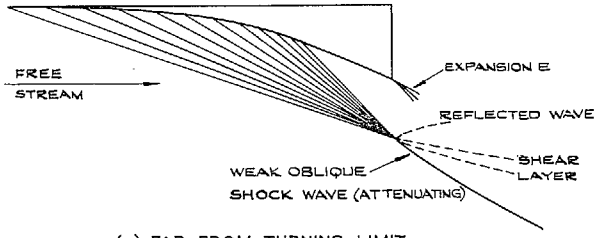

(a) FAR FROM TURNING LIMIT.

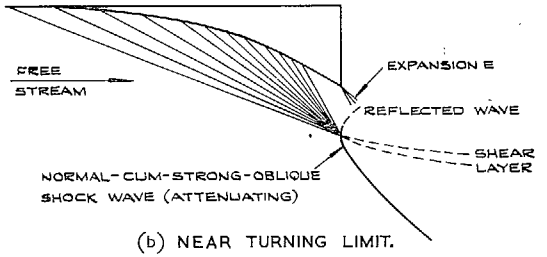

(b) NEAR TURNING LIMIT.

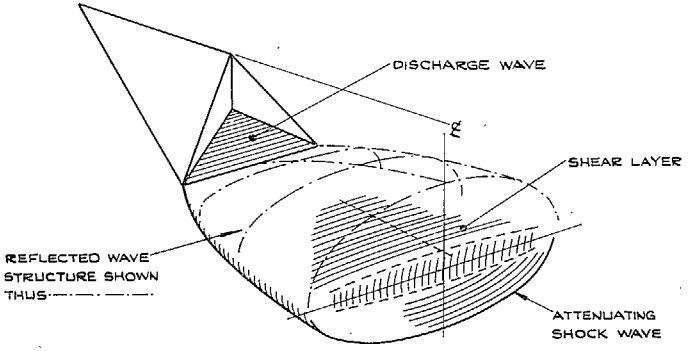

(c) SHOCK SYSTEM FOR COMPLETE BODY.

FIG. 18a to c. Possible trailing shock systems for caret bodies producing centred compression.

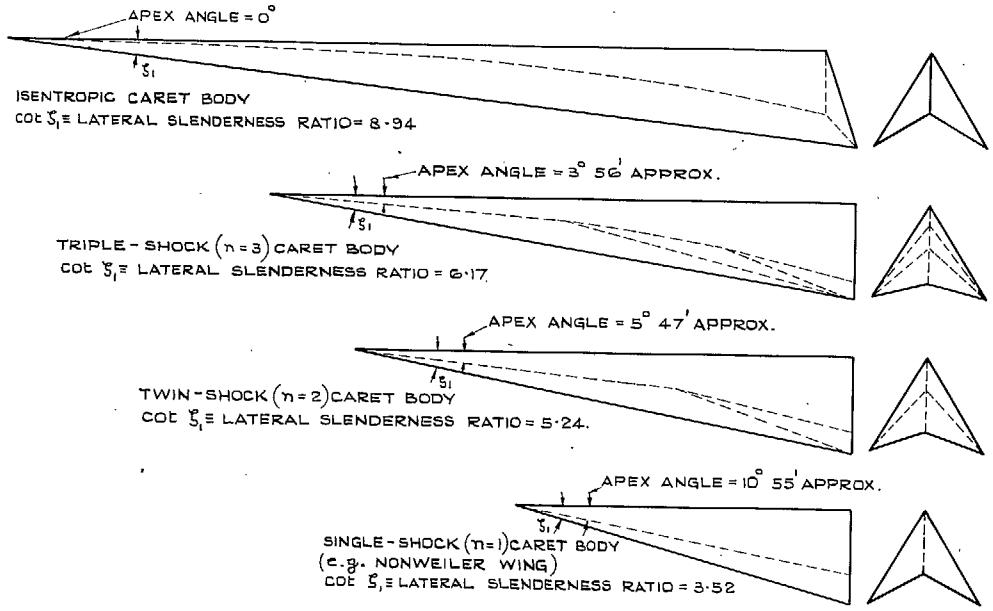

FIG. 19. Isentropic and multi- and single-shock caret bodies designed for free-stream and discharge Mach numbers (M_∞ and M_{comp}) of 9 and 6.

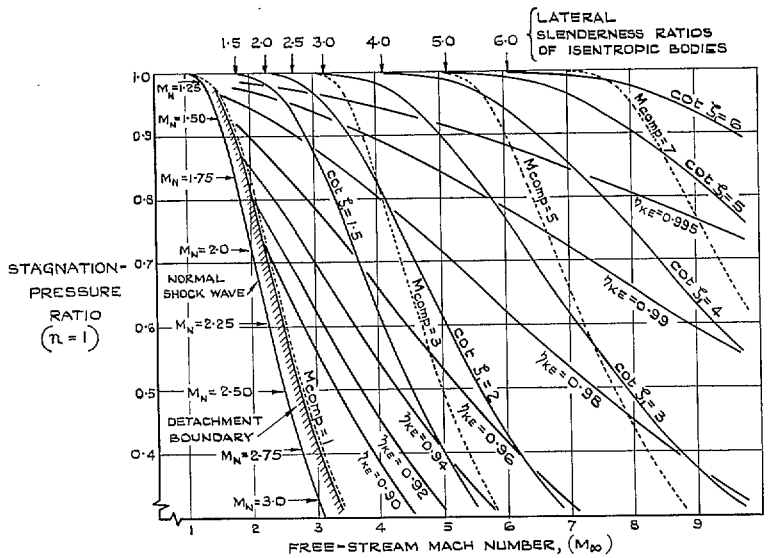

(a) SINGLE-SHOCK CARET BODIES, n=1 (E.G. NONWEILER WINGS).

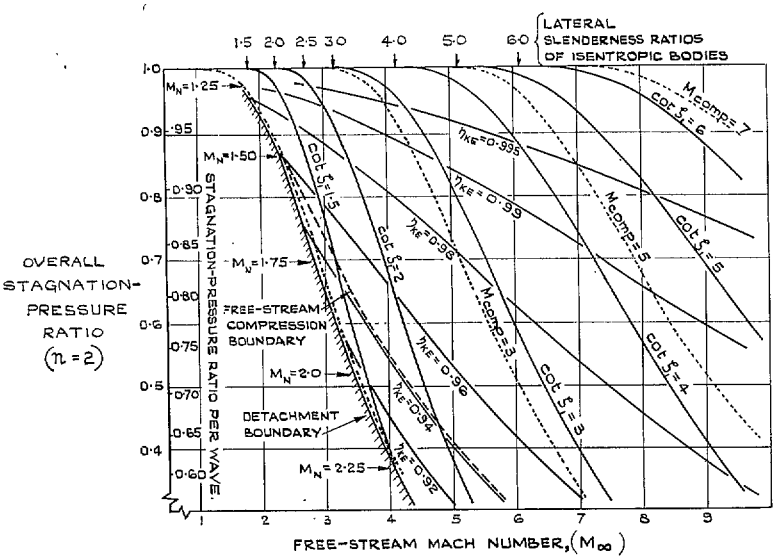

(b) CARET BODIES HAVING TWO EQUAL SHOCK WAVES, n=2.

FIG. 20a and b. Features of *n*-wave centred compression flows.

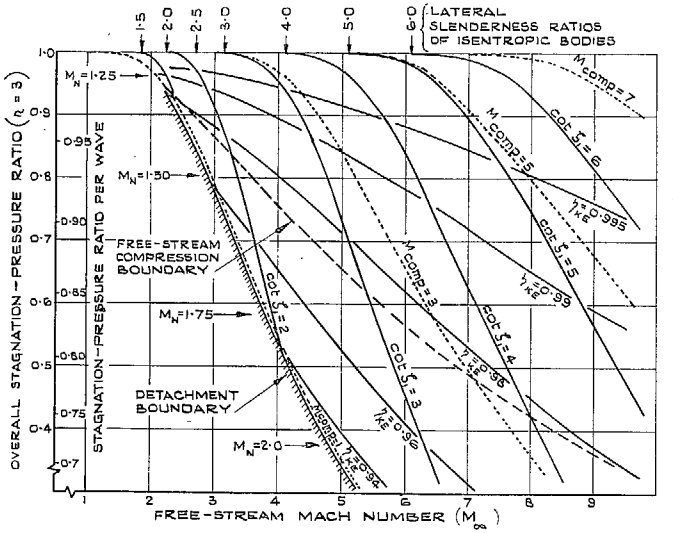

(c) CARET BODIES HAVING THREE EQUAL SHOCK WAVES, n = 3.

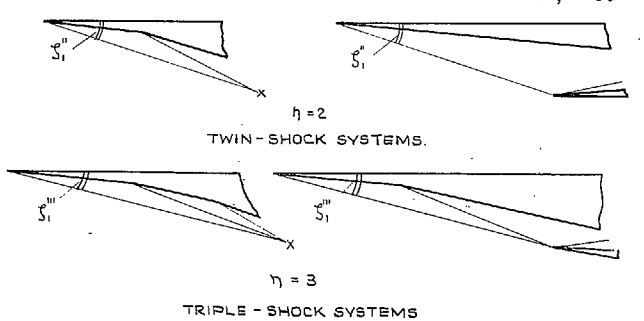

(d) ALTERNATIVE WAVE CONFIGURATIONS (REFER ALSO TO FIG. 19).

FIG. 20c and d. Features of *n*-wave centred compression flows.

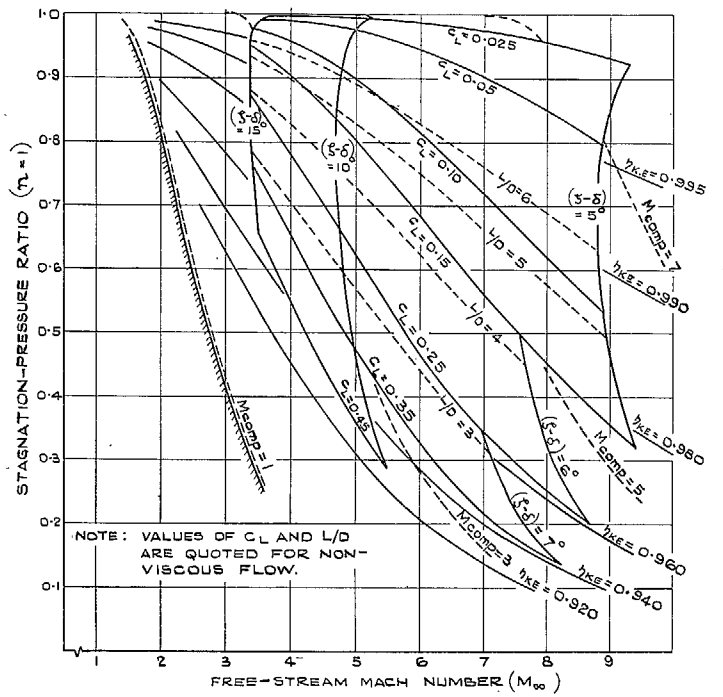

NOTE: IF VISCOUS FORCES ARE IGNORED,

THEN $C_{L_{\text{NON-VISCOUS}}} = \dfrac{\text{LIFT FROM PRESSURE ON LOWER SURFACE,}}{\tfrac{1}{2}\gamma_\infty M_\infty^2 \cdot p_\infty \cdot S}$,

(WHERE, FOR CARET BODY SHOWN,
S = PROJECTED AREA OF △OBC ON THE PLANE THROUGH OA AND PARALLEL TO BC)
AND ALSO, $(L/D)_{\text{NON-VISCOUS}} = \cot\delta$.

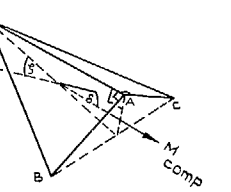

FIG. 21. Variation with free-stream Mach number of the non-viscous lift and drag, and of the aerodynamic efficiency of single-shock caret bodies.

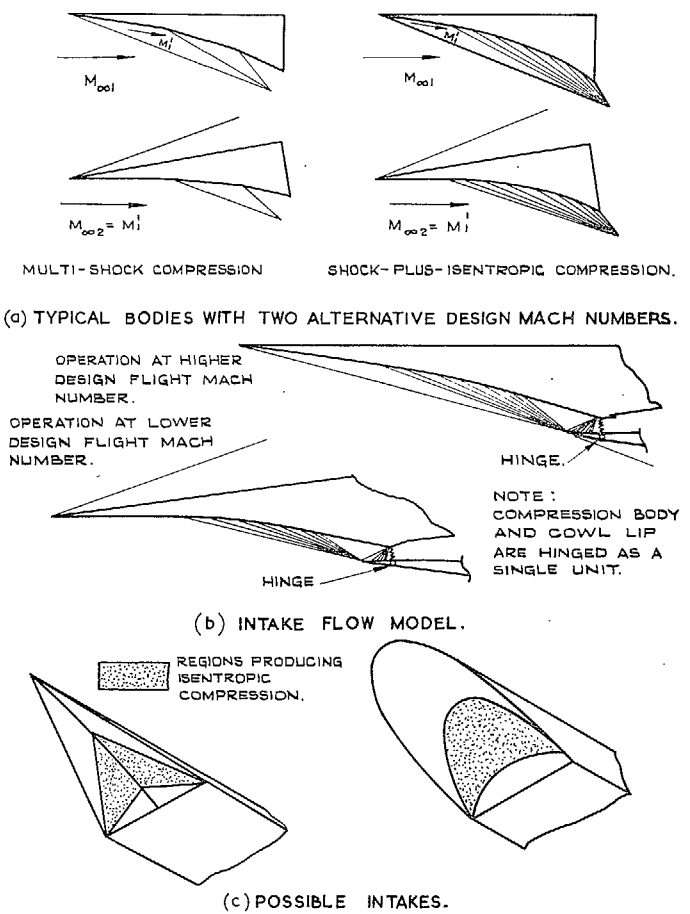

FIG. 22a to c. Double 'design Mach number' feature of some bodies producing centred compression, and application to intakes.

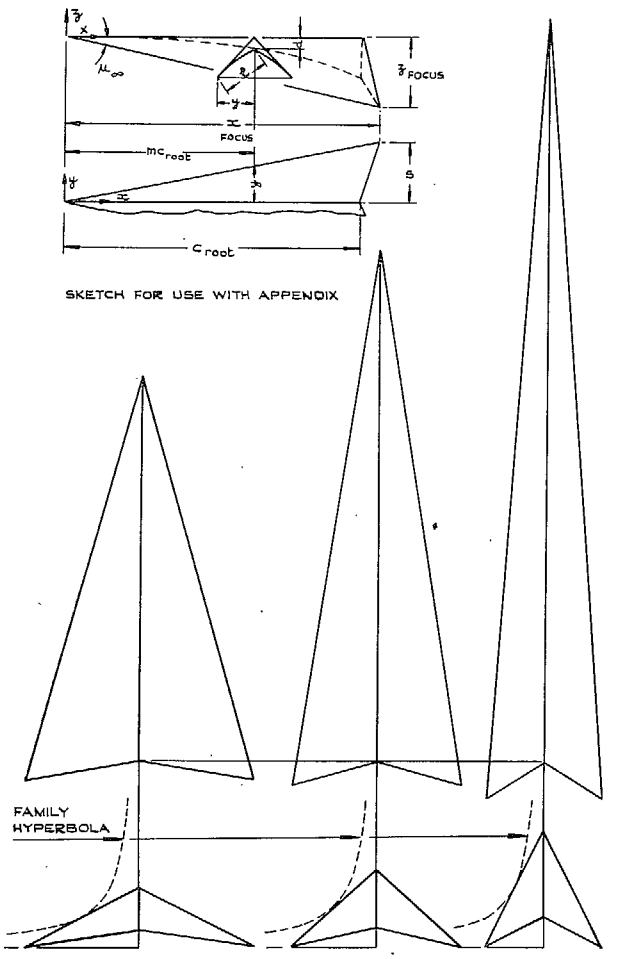

FIG. 23. Family of isentropic caret bodies, designed for the same values of M_∞ and M_{comp}, and for the same mass flows.

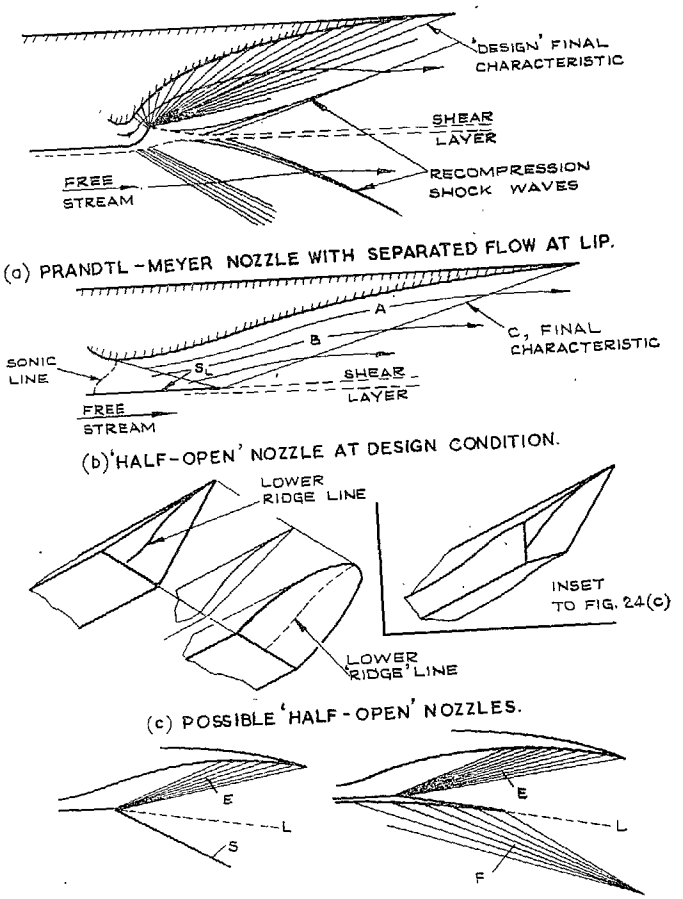

FIG. 24a to d. Nozzles and exhaust flows.

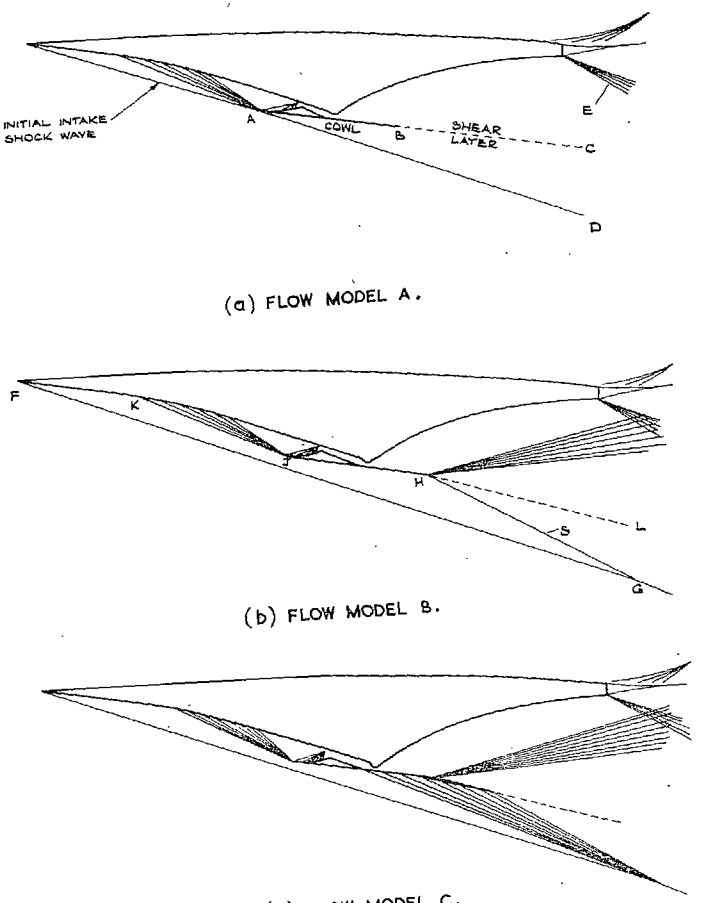

FIG. 25a to c. Lifting-cum-propulsive flow models.

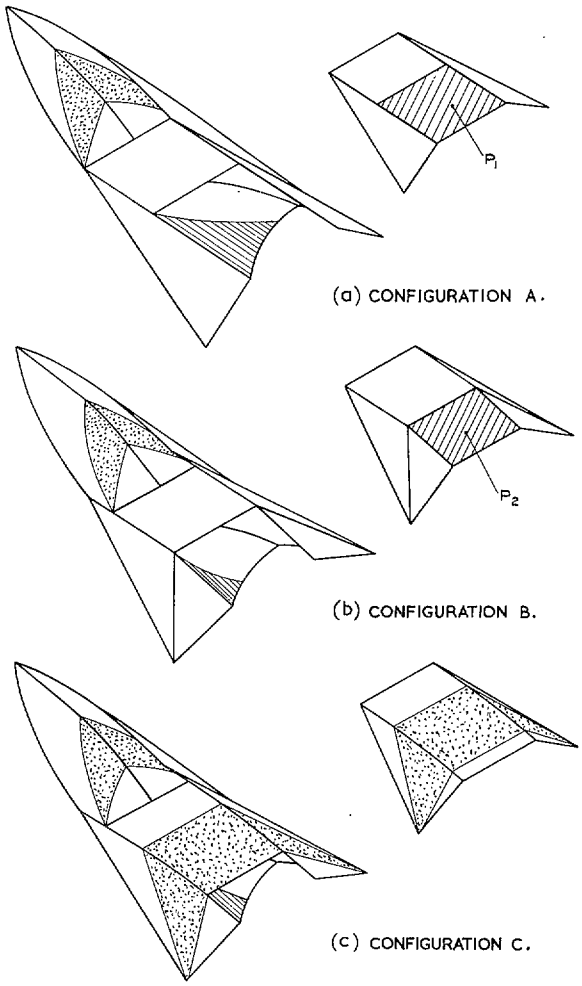

FIG. 26a to c. Integrated configurations.

(90172) Wt. 66/2301 K.5 9/64 Hw.

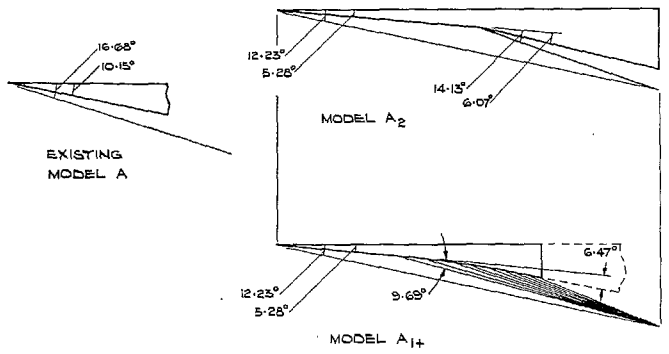

(a) FLOW MODELS FOR FREE-STREAM AND DISCHARGE MACH NUMBERS OF 6·85 AND 5·12(8) (NOT RECOMMENDED FOR TEST).

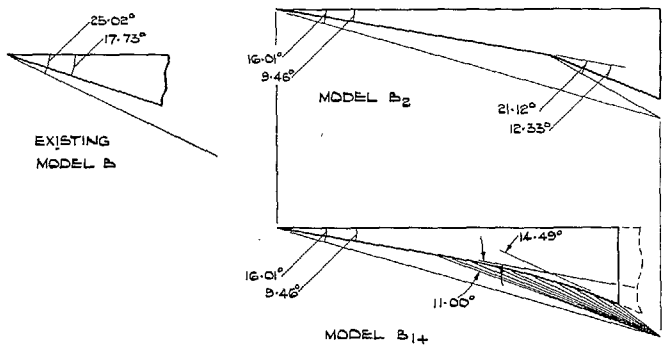

(b) FLOW MODELS FOR FREE-STREAM AND DISCHARGE MACH NUMBERS OF 6·85 AND 3·91(2) (RECOMMENDED FOR TEST).

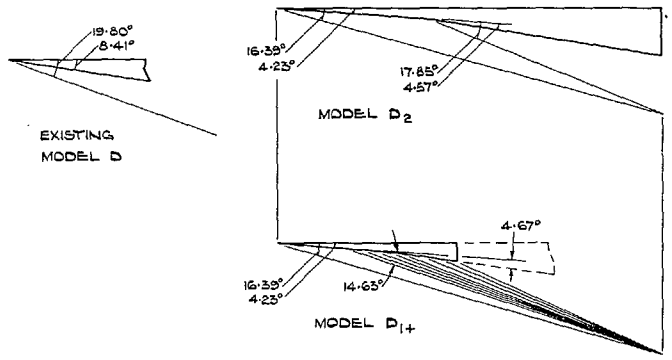

(c) FLOW MODELS FOR FREE-STREAM AND DISCHARGE MACH NUMBERS OF 4·30 AND 3·63(1) (MODEL D_2 NOT RECOMMENDED FOR TEST; BUT MODEL D_{1+} POSSIBLY SUITABLE FOR TEST).

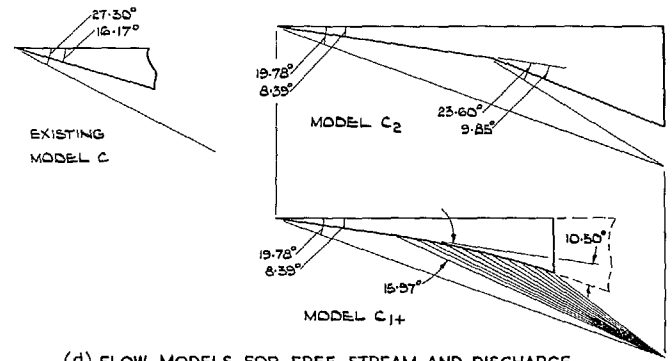

(d) FLOW MODELS FOR FREE-STREAM AND DISCHARGE MACH NUMBERS OF 4·30 AND 3·01(8) (RECOMMENDED FOR TEST).

FIG. 27a to d. Possible variants of existing models in current wind-tunnel programme.

Publications of the Aeronautical Research Council

ANNUAL TECHNICAL REPORTS OF THE AERONAUTICAL RESEARCH COUNCIL (BOUND VOLUMES)

1942 Vol. I. Aero and Hydrodynamics, Aerofoils, Airscrews, Engines. 75*s.* (post 2*s.* 9*d.*)
Vol. II. Noise, Parachutes, Stability and Control, Structures, Vibration, Wind Tunnels. 47*s.* 6*d.* (post 2*s.* 3*d.*)

1943 Vol. I. Aerodynamics, Aerofoils, Airscrews. 80*s.* (post 2*s.* 6*d.*)
Vol. II. Engines, Flutter, Materials, Parachutes, Performance, Stability and Control, Structures. 90*s.* (post 2*s.* 9*d.*)

1944 Vol. I. Aero and Hydrodynamics, Aerofoils, Aircraft, Airscrews, Controls. 84*s.* (post 3*s.*)
Vol. II. Flutter and Vibration, Materials, Miscellaneous, Navigation, Parachutes, Performance, Plates and Panels, Stability, Structures, Test Equipment, Wind Tunnels. 84*s.* (post 3*s.*)

1945 Vol. I. Aero and Hydrodynamics, Aerofoils. 130*s.* (post 3*s.* 6*d.*)
Vol. II. Aircraft, Airscrews, Controls. 130*s.* (post 3*s.* 6*d.*)
Vol. III. Flutter and Vibration, Instruments, Miscellaneous, Parachutes, Plates and Panels, Propulsion. 130*s.* (post 3*s.* 3*d.*)
Vol. IV. Stability, Structures, Wind Tunnels, Wind Tunnel Technique. 130*s.* (post 3*s.* 3*d.*)

1946 Vol. I. Accidents, Aerodynamics, Aerofoils and Hydrofoils. 168*s.* (post 3*s.* 9*d.*)
Vol. II. Airscrews, Cabin Cooling, Chemical Hazards, Controls, Flames, Flutter, Helicopters, Instruments and Instrumentation, Interference, Jets, Miscellaneous, Parachutes. 168*s.* (post 3*s.* 3*d.*)
Vol. III. Performance, Propulsion, Seaplanes, Stability, Structures, Wind Tunnels. 168*s.* (post 3*s.* 6*d.*)

1947 Vol. I. Aerodynamics, Aerofoils, Aircraft. 168*s.* (post 3*s.* 9*d.*)
Vol. II. Airscrews and Rotors, Controls, Flutter, Materials, Miscellaneous, Parachutes, Propulsion, Seaplanes, Stability, Structures, Take-off and Landing. 168*s.* (post 3*s.* 9*d.*)

1948 Vol. I. Aerodynamics, Aerofoils, Aircraft, Airscrews, Controls, Flutter and Vibration, Helicopters, Instruments, Propulsion, Seaplane, Stability, Structures, Wind Tunnels. 130*s.* (post 3*s.* 3*d.*)
Vol. II. Aerodynamics, Aerofoils, Aircraft, Airscrews, Controls, Flutter and Vibration, Helicopters, Instruments, Propulsion, Seaplane, Stability, Structures, Wind Tunnels. 110*s.* (post 3*s.* 3*d.*)

Special Volumes

Vol. I. Aero and Hydrodynamics, Aerofoils, Controls, Flutter, Kites, Parachutes, Performance, Propulsion, Stability. 126*s.* (post 3*s.*)
Vol. II. Aero and Hydrodynamics, Aerofoils, Airscrews, Controls, Flutter, Materials, Miscellaneous, Parachutes, Propulsion, Stability, Structures. 147*s.* (post 3*s.*)
Vol. III. Aero and Hydrodynamics, Aerofoils, Airscrews, Controls, Flutter, Kites, Miscellaneous, Parachutes, Propulsion, Seaplanes, Stability, Structures, Test Equipment. 189*s.* (post 3*s.* 9*d.*)

Reviews of the Aeronautical Research Council

1939–48 3*s.* (post 6*d.*) 1949–54 5*s.* (post 5*d.*)

Index to all Reports and Memoranda published in the Annual Technical Reports

1909–1947 R. & M. 2600 (out of print)

Indexes to the Reports and Memoranda of the Aeronautical Research Council

Between Nos. 2351–2449	R. & M. No. 2450	2*s.* (post 3*d.*)
Between Nos. 2451–2549	R. & M. No. 2550	2*s.* 6*d.* (post 3*d.*)
Between Nos. 2551–2649	R. & M. No. 2650	2*s.* 6*d.* (post 3*d.*)
Between Nos. 2651–2749	R. & M. No. 2750	2*s.* 6*d.* (post 3*d.*)
Between Nos. 2751–2849	R. & M. No. 2850	2*s.* 6*d.* (post 3*d.*)
Between Nos. 2851–2949	R. & M. No. 2950	3*s.* (post 3*d.*)
Between Nos. 2951–3049	R. & M. No. 3050	3*s.* 6*d.* (post 3*d.*)
Between Nos. 3051–3149	R. & M. No. 3150	3*s.* 6*d.* (post 3*d.*)

HER MAJESTY'S STATIONERY OFFICE

from the addresses overleaf

Printed and published by
HER MAJESTY'S STATIONERY OFFICE

To be purchased from
York House, Kingsway, London W.C.2
423 Oxford Street, London W.1
13A Castle Street, Edinburgh 2
109 St. Mary Street, Cardiff
39 King Street, Manchester 2
50 Fairfax Street, Bristol 1
35 Smallbrook, Ringway, Birmingham 5
80 Chichester Street, Belfast 1
or through any bookseller

Printed in England

S.O. Code No. 23-3383